Electrochemical degradation of antibiotics using flow-through graphene sponge electrodes

Natalia Ormeno-Cano[a,b], Jelena Radjenovic [a,c]*

[a]Catalan Institute for Water Research (ICRA-CERCA), c/Emili Grahit, 101, 17003 Girona, Spain

[b]University of Girona, Girona, Spain

[c]Catalan Institution for Research and Advanced Studies (ICREA), Passeig Lluís Companys 23, 08010 Barcelona, Spain

* Corresponding author:

Jelena Radjenovic, Catalan Institute for Water Research (ICRA), Scientific and Technological Park of the University of Girona, 17003 Girona, Spain

Phone: + 34 972 18 33 80; Fax: +34 972 18 32 48; E-mail: jradjenovic@icra.cat

Abstract

Graphene sponge electrodes doped with atomic boron and nitrogen were employed for electrochemical degradation of antibiotics sulfamethoxazole, trimethoprim, ofloxacin, and erythromycin. The removal of antibiotics that displayed strong π-π interactions (i.e., ofloxacin) with reduced graphene oxide (RGO) coating was less limited by the mass transfer and removal efficiencies >80% were observed for the investigated range of electrolyte flowrates. At the highest applied flowrate (700 LMH), increase in the anodic current significantly worsened the removal of trimethoprim and erythromycin due to the detrimental impact of the evolving gas bubbles. Increase in current at 700 LMH led to a stepwise increase in the removal efficiency of sulfamethoxazole due to its enhanced electrosorption. Electrochemical degradation was achieved via ozone, hydrogen peroxide and hydroxyl radical ($^{\bullet}OH$). Extraction of the employed graphene sponges confirmed the degradation of the strongly adsorbing antibiotics. Identified electrochemical transformation products of erythromycin confirmed the participation of $^{\bullet}OH$, through N-demethylation of the dimethylamine group. In real tap water, removal efficiencies were lower for all target antibiotics. Lower electric conductivity of tap water and thus increased thickness of the electric double layer likely limited their interaction with the graphene sponge surface, in addition to the presence of low amounts of organic matter.

Keywords: fluoroquinolone, macrolide, sulfonamide, trimethoprim, reduced graphene oxide

Introduction

Widespread use of antibiotics in human and veterinary medicine has led to their frequent detection in soil (O'Connor and Aga, 2007), groundwater (Ma et al., 2015), surface water (Yang et al., 2020), and even tap water (Ben et al., 2020; Carvalho and Santos, 2019; Yang et al., 2020). Over the past decades, it has become increasingly clear that the spread of antimicrobial resistance is one of the major challenges of the 21st century. According to the latest report of the United Nations (UN), at least 700,000 people die each year due to drug-resistant diseases (Bryan-Wilson, 2016). Traditional biological wastewater treatment plants are not capable of degrading antibiotics, and thus contribute to the development of antibiotic resistance in the receiving water bodies (Cacace et al., 2019; Carvalho and Santos, 2019; Pruden et al., 2012). Due to their prevalence in the environment, antibiotics and antibiotic resistant genes (ARGs) were detected in the treated drinking water worldwide (Ben et al., 2020; Khan et al., 2016). Although home water purification systems are often used to improve the quality of tap water, recent study demonstrated the increase in the concentrations of antibiotics and ARGs during long-term (i.e., > three months) usage of different filtration devices, due to the development of a biofilm (Gu et al., 2021).

Electrochemical treatment systems have been gaining increasing attention for decentralized and distributed treatment of contaminated water because of their small footprint, modular design, easy automation and no requirement for chemical addition due to the *in situ* formation of strong oxidant species such as hydroxyl radical ($^{•}OH$), hydrogen peroxide (H_2O_2), ozone (O_3), and others (Radjenovic and Sedlak, 2015). Different anode materials such as boron-doped diamond (BDD) (Mordačíková et al., 2020), Magnéli

phase Ti_4O_7 (Liang et al., 2018), and mixed metal oxide (MMO) anodes $Ti/RuIrO_2$ (Radjenovic et al., 2011), Ti/RuO_2 (Kaur et al., 2019), Ti/SnO_2-Sb (Chaplin, 2014) have been investigated for the degradation of antibiotics and other persistent contaminants. All of the above mentioned electrode materials suffer from a major limitation: production of chlorine in the presence of chloride, and in the case of highly oxidizing anodes (BDD, Ti_4O_7, Ti/SnO_2-Sb), further oxidation of chloride to chlorate (ClO_3^-) and perchlorate (ClO_4^-) (Chaplin, 2019; Radjenovic and Sedlak, 2015). Chlorinated organic byproducts formed by the reaction of chlorine with the organic matter may be partially removed by an activated carbon post-treatment. Yet, toxic, and persistent chlorate and perchlorate are extremely challenging to eliminate and there is no platform technology for their removal from water. Minimization of the production of organochlorines, ClO_3^- and ClO_4^- during electrooxidation has become one of the greatest challenges in the search for a safer and more efficient electrochemical water treatment system.

Recently developed graphene-based sponge electrodes overcome this limitation, as they do not form any chlorate and perchlorate when polarized at high anodic current densities, whereas the current efficiency for free chlorine generation is <0.1% even in the presence of 20 mM NaCl solutions (Baptista-Pires et al., 2021). The developed bottom-up synthesis method allows constructing a structurally stable, three-dimensional (3D) material using mineral wool as template, and easy functionalization of the reduced graphene oxide (RGO) coating by different dopants and thus tailoring of its electrocatalytic activity. Furthermore, the anodically polarized graphene sponge electrode showed exceptional electrochemical stability without corrosion typically observed for graphite and carbon-based materials (Baptista-Pires et al., 2021; Norra et al., 2022), presumably due to the formation of covalent C-Si and C-O bonds between the

nanocoating of RGO and SiO_2 (major component of the mineral wool template), as predicted by the density functional theory (DFT) modelling (Ramezanzadeh et al., 2016; Shemella and Nayak, 2009; Su et al., 2019). Another important advantage of the developed graphene sponge electrodes is the very low cost of their synthesis, estimated at less than €50 per m^2 of the material projected surface area (Baptista-Pires et al., 2021; Norra et al., 2022).

In this study, we investigated the performance of a flow-through electrochemical system equipped with boron-doped reduced graphene oxide (BRGO) sponge anode and nitrogen-doped RGO (NRGO) sponge cathode for the removal of a set of antibiotics from water, namely sulfamethoxazole (SMX), ofloxacin (OFX), erythromycin (ERT), and trimethoprim (TMP). They were selected as representative of the most widely used groups of antibiotics, i.e., sulfonamides (SMX), which are often administered with TMP in veterinary medicine, fluoroquinolones (OFX) and macrolides (ERT), which are often detected in wastewater effluents (Sabri et al., 2020), groundwater (Boy-Roura et al., 2018)), and even drinking water resources (Watkinson et al., 2009), often leading to the presence of relevant antibiotic resistance genes in tap water (Su et al., 2018). N-doping was implemented to catalyze the *in situ* production and activation of H_2O_2 to $^{\bullet}OH$ radicals at NRGO cathode (Su et al., 2019). B-doping was used to enhance the electrogeneration of O_3 and improve the electrocatalytic activity of the anodically charged graphene sponge electrode (Baptista-Pires et al., 2021; Zhang et al., 2020). Electrochemical degradation of antibiotics was studied in a one-pass, continuous mode at different applied currents and flowrates, and using low conductivity supporting electrolyte (i.e., 1 mS cm^{-1}) to investigate the reactor performance under the challenging conditions of high ohmic drop, which will occur for most contaminated waters. We have further evaluated the

electrochemical degradation of antibiotics by: *i)* pre-loading of the graphene sponge electrodes with the target antibiotics, and posterior current application, and *ii)* comparison of the remaining amount of antibiotics adsorbed onto the graphene sponge electrodes operated with and without the application of current. The proof-of-concept study was also performed using real tap water amended with the target antibiotics. Finally, to gain insight into the main oxidant species involved, elucidation of transformation products was performed using ERT as a model contaminant.

Materials and methods

Graphene sponge synthesis

BRGO and NRGO sponges were synthesized using the previously developed protocol, slightly modified to simplify the synthesis procedure (Norra et al., 2022). The scheme of the synthesis procedure is illustrated in **Figure S1**. In brief, GO solutions (2 g L^{-1}) were prepared from commercial graphene oxide (Graphenea, Spain) and mixed with boric acid (42.86 g L^{-1}) and urea (300 g L^{-1}) to synthesize BRGO and NRGO sponge, respectively. A commercial sample of mineral wool (Diaterm, Spain) was used as a template for the graphene sponge synthesis. Mineral wool was soaked with the prepared GO solution and placed in a hydrothermal reactor for 12 h treatment at 180°C. The resulting graphene-based sponges were thoroughly cleaned with MilliQ water to remove the excess (unbonded) RGO and connected to the stainless-steel current feeders for their use in electrochemical flow-through reactor. Detailed surface characteristics of the BRGO and NRGO sponges, including scanning electron microscopy (SEM), X-ray photoelectron spectroscopy (XPS), X-ray diffraction **(XRD),** Raman spectroscopy, contact angle measurement, Brunauer–Emmett–Teller (BET) specific surface areas, and zeta potential

measurements of the employed graphene sponge electrodes are given in (Baptista-Pires et al., 2021; Norra et al., 2022) and summarized in the **Text S1**.

Experimental set-up

Cylindrical flow-through reactor equipped with the BRGO anode and NRGO cathode (17.34 cm^2 projected surface area each) was operated in one-pass, continuous mode at varying flowrates of 2.5, 5, 10 and 20 mL min^{-1} (i.e., effluent fluxes of 87.5, 175, 300 and 700 L m^{-2} h^{-1} (LMH), and hydraulic retention times (HRTs) of 7, 3.5, 1.7 and 0.88 min, respectively), controlled by a digital gear pump (Cole-Parmer, USA) (**Figure S3**). The flow direction was BRGO anode (A)- NRGO cathode (C), which was determined as more efficient for the removal of organic and microbial contaminants in our previous studies (Baptista-Pires et al., 2021). Direct current was applied to the BRGO anode (working electrode) using a BioLogic multi-channel potentiostat/galvanostat VMP-300 and a leak-free Ag/AgCl reference electrode (Harvard Apparatus) sandwiched between the BRGO anode and NRGO cathode and isolated using polypropylene meshes to prevent short circuiting. Target antibiotics were added at low concentration (0.2 µM) to a 10 mM phosphate buffer (NaH$_2$PO$_4$/Na$_2$HPO$_4$, electric conductivity 1 mS cm^{-1}) to investigate the system performance under realistic conditions of water treatment, where ohmic drop represents a major challenge. The reactor was operated in chronopotentiometric mode at different anodic currents. The impact of current was evaluated for the lowest (87.5 LMH) and the highest (700 LMH) applied flux at 50, 150, 250 mA of applied anodic current (geometric current densities of 29, 86 and 144 A m^{-2}, respectively). Proof-of-concept experiments were performed using real tap water (0.4-0.5 mS cm^{-1}) amended with the target antibiotics at 0.2 µM, in chronopotentiometric mode at 150 mA of applied anodic current (86 A m^{-2}). To evaluate the loss of the target antibiotics due to their adsorption

onto the graphene sponges, all experiments were first conducted in the open circuit (OC) mode, without the application of current. At the end of each run, samples were taken after the current was switched off (OC$_{final}$), to evaluate if the removal of antibiotics during the application of current occurred only due to electrosorption, or also electrodegradation. If the concentrations in OC$_{final}$>OC, this would indicate that a fraction of a target contaminant was only electrosorbed. To further evaluate the impact of the current on the antibiotics removal, graphene sponges were first operated in OC mode during 48 h and using a low flow rate (i.e., 87.5 LMH), to allow the adsorption of antibiotics onto the sponges. The partially saturated sponges were then employed for electrochemical removal of antibiotics at 144 A m^{-2} of applied current. To verify the degradation of the adsorbed antibiotics, BRGO and NRGO sponges employed for electrochemical degradation of antibiotics (i.e., 144 A m^{-2}, 28 h run, 0.2 µM of target antibiotics in 10 mM phosphate buffer, 175 LMH) were extracted with methanol, and the concentration of the target antibiotics in the extract was determined by applying appropriate dilutions with MilliQ water and analyzing them as explained further in the text. These concentrations were compared with the concentrations of extracts obtained from the BRGO and NRGO sponges employed in the reactor operated in the OC mode only under identical conditions but without applying the current (i.e., OC, 28 h, 0.2 µM of target antibiotics in 10 mM phosphate buffer, 175 LMH). The ohmic drop, ΔE_{ohmic}, and the correction of the anode potentials was conducted using electrochemical impedance spectroscopy (EIS). The EIS experimental data was fitted using the BioLogic EC-lab software, as described in the **Text S2**. Anode potentials were expressed versus Standard Hydrogen Electrode (/SHE, V). All results are expressed as mean values of triplicate experiments, with their standard deviations (SDs).

The electrical energy per order (E_{eo}, kWh m^{-3}) was calculated according to the equation (Radjenovic and Sedlak, 2015):

$$E_{EO} = \frac{P}{q.log\frac{C_o}{C}} \qquad \text{(eq. 1)}$$

where P is the rated power of the system (kW), q is the water flowrate (m^3 h^{-1}), and C_0 and C are the influent and effluent contaminant concentrations (µM, note that for an order of magnitude removal, log C/C_0=1). The production of ozone and hydrogen peroxide was determined at the highest currents applied in 10 mM phosphate buffer and tap water of 144 A m^{-2} and 86 A m^{-2}, respectively. The formation of ozone was evaluated in C-A flow direction (anodically generated, to avoid the loss of ozone at the cathode), whereas H$_2$O$_2$ was determined in the A-C flow direction (cathodically generated). The production of $^\bullet$OH was also evaluated in the selected A-C flow direction at 144 A m^{-2} (10 mM phosphate buffer) and 86 A m^{-2} (tap water) using terephthalic acid (TA) as a probe compound at the initial concentration of 0.12 mM. TA is well suited as a probe compound for electrochemically generated OH$^\bullet$ because it does not undergo direct electrolysis and has very low reactivity with ozone (Jing and Chaplin, 2017).. The current efficiency CE (%) of the oxidant species produced were evaluated according to **Text S4**.

Study of the transformation products of ERT

To gain insight into the electrochemical degradation mechanisms occurring at the graphene sponge electrodes, experiments targeting the identification of transformation products (TPs) were performed using ERT a model compound at high initial concentration (20 µM in 10 mM phosphate buffer, pH 7-7.2), to allow the detection of TPs in the full-scan exploration mode. The reactor was operated at 144 A m^{-2} of applied anodic current and an effluent flux of 175 LMH. To differentiate the TPs formed at the BRGO anode and NRGO cathode, sampling was conducted after the anode by adding a

sampling syringe between the electrodes, and at the exit of the electrochemical reactor (i.e., after the NRGO cathode). The metal sampling syringe was isolated with the fine polypropylene meshes to avoid short-circuiting between the electrodes, and the samples were taken at 10, 20 and 30 bed volumes.

Analytical methods

Samples from the flow-through reactor were analyzed using ultraperformance liquid chromatography (UPLC, Waters, USA) with an Acquity UPLC HSS T3 column (2.1×50 mm, 1.8 μm, Waters), coupled to quadrupole linear ion trap mass spectrometer (QqLIT-MS) with a turbo Ion Spray source (5500 QTRAP, Applied Biosystems, USA). Details of the analytical method employed for the analysis of target antibiotics in multiple reaction monitoring (MRM) mode are summarized in **Text S3** and **Table S1**. Tentative identification of TPs of ERT was performed by full-scan mode of analysis, isolation of the protonated molecular ions, collision induced dissociation (CID) MS^2 experiments in (+)ESI mode and mass spectral comparison with the parent compound, as well as with the literature data. The concentrations of ozone and H_2O_2 were measured for the reactor effluent samples immediately after sampling. H_2O_2 was measured with a spectrophotometric method, using 0.01 M $CuSO_4$ solution and 0.1% w/v 2,9 dimethyl-1,10-phenanthroline (DMP) solution, based on the formation of $Cu(DMP)^{2+}$ that shows an absorption maximum at 454 nm (Baptista-Pires et al., 2021). Ozone (in the absence of chlorine) was measured using a colorimetric method with N,N-diethyl-p-phenylenediamine (DPD), using Chlorine/Ozone/Chlorine dioxide cuvette tests LCK 310 (Hach Lange, Spain) were employed. TA was determined using high performance liquid chromatography (HPLC) – ultraviolet (UV) spectroscopy (Agilent Technologies 1200 series) at 239 nm (quantification limit of 1.98 mg L^{-1}).

Results and discussion

SEM analysis of the synthesized BRGO and NRGO sponges was performed to ensure an even coating of the mineral wool template and the presence of wrinkled graphene sheets on its surface and is presented in **Figure S2**. The results of other surface characterization techniques employed are summarized in **Text S1**.

Electrochemical removal of antibiotics: impact of anodic current, flowrate and compound properties

Given the different physico-chemical properties of the target antibiotics (e.g., log D, pKa, **Table S2**), the performance of graphene-based sponge electrodes in the OC mode was varying from very limited adsorption as was the case of SMX, to a near complete adsorption onto the graphene sponge electrodes regardless of the employed flowrate in the case of OFX. **Figure 1** summarizes the observed removals of the target antibiotics in the OC and at the highest applied current (144 A m^{-2}), obtained in steady state (i.e., at constant effluent concentrations) at varying flowrates. Only up to 10% of SMX was removed due to adsorption onto the sponges in the OC (at the lowest applied flux of 87.5 LMH). Previously, RGO in suspension was determined to have high adsorption affinity for SMX (Wang et al., 2017). Nevertheless, variations in the RGO wrinkling have a pronounced effect on the energy distribution of its adsorption sites (Bai et al., 2013). Graphene sponges with stacked RGO sheets exhibited very low adsorption affinity towards SMX. This can be explained by the high polarity of SMX (log D= -0.56, **Table S2**) and its negative charge in the experimental pH 7-7.2 (pKa$_1$=1.4, pKa$_2$=5.8, **Table S2, Figure S5**). Given that the zeta-potentials of both BRGO and NRGO sponges are negative at pH 7 (i.e., –36.2 mV and –13.3 mV, respectively, **Text S1**), SMX anion is

electrostatically repulsed by the graphene-based sponge surface. In the OC, increasing the flowrate had a clear detrimental effect on the removal of ERT, which was decreased from 86.4% (87.5 LMH) to 60% (700 LMH) (**Figure 1A**). Macrolide antibiotics have no aromatic rings and do not undergo π-π interactions. The interaction of the positively charged ERT with the graphene sponges was dominated by the weaker cation-π interactions, i.e., electrostatic attraction between the positively charged dimethylamine group of ERT and the electron-rich π system of the RGO coating (Zhao and Zhu, 2020). Also, ERT was the only antibiotic with the positive log D value at pH 7 (log D = 1.69, **Table S2**) and may have interacted with the graphene sponge surface via hydrophobic interactions. In the case of TMP (uncharged at pH 7), its removal due to adsorption in the OC was decreased from 96% (87.5 LMH) to 86.4% (700 LMH). Previously, strong π-π interactions were determined as the dominant adsorption mechanism of an uncharged TMP molecule at RGO and N-doped RGO (Carrales-Alvarado et al., 2020), thus its adsorption was significant even at the highest applied flowrate. Finally, 90-97% of OFX was adsorbed onto the graphene sponges and its removal was not affected by the electrolyte flowrate in the investigated range. Even though the log D value of OFX (-2.08, **Table S2**) indicates a highly polar compound, it is adsorbed onto the graphene-based materials via strong π-π electron donor-acceptor interactions, similar to other contaminants with multiple aromatic ring structures (Baptista-Pires et al., 2021; Zhang et al., 2020). In addition, OFX interacts with the graphene-based materials via hydrogen bonding with the oxygen functional groups of the RGO (Ehtesabi et al., 2019), as well as cation-π interactions via its positively charged tertiary amine group (OFX is present as zwitterion at pH 7, **Figure S5**).
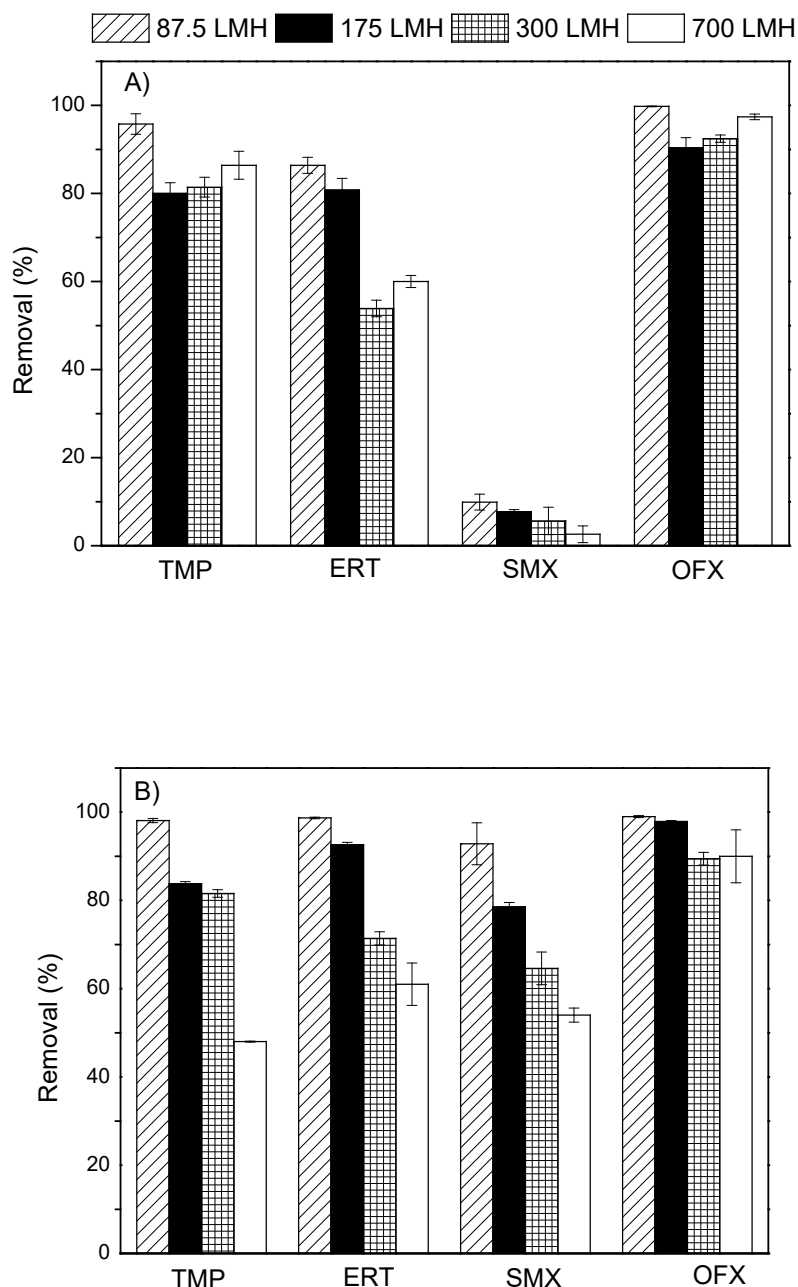
Figure 1 Removal (%) of TMP, SMX, ERT and OFX at varying flow rates using 10 mM phosphate buffer, pH 7: A) in the open circuit (OC), and B) at 250 mA of applied anodic current (144 A m^{-2}).

At the lowest applied flux of 87.5 LMH, the impact of the applied current on the removal efficiencies of the target antibiotics could not be observed and near complete removals were noted for all investigated conditions (**Figure S6**). Although pronounced adsorption of target antibiotics makes the elucidation of the impact of current and their

14

electrochemical degradation difficult, it may represent an advantage as their removal is less limited by the mass transfer, provided that the adsorbed contaminant is further electrochemically degraded and thus there is no passivation of the electrode surface. At 700 LMH, stepwise increase in the anodic current from 29 to 86 and 144 A m^{-2} led to a gradual increase in the removal of SMX, from 28% to 42% and 54%, respectively. However, higher currents had a detrimental impact on the removal of ERT, TMP, and to some degree OFX (**Figure S6**). This is likely due to the increased production of oxygen and hydrogen bubbles and thus more limited interaction of the target antibiotics with the graphene sponge surface. At 700 LMH and 144 A m^{-2}, the reactor had difficulties reaching steady state due to the accumulation of bubbles, and the presented removals for target antibiotics for this experiment (white bars in **Figure 1A**) represent mean values of the removals obtained for the first 30 bed volumes. Better removal of the negatively charged SMX at higher currents may be due to its enhanced electrosorption at the positively charged BRGO anode, and its subsequent degradation by the electrogenerated oxidant species (e.g., O_3, $^{\bullet}OH$), as discussed further in the text. Electrosorption onto the BRGO anode was not relevant for the removal of TMP (uncharged, π-π interactions), OFX (zwitterion, π-π interactions) and ERT (positively charged, cation-π interactions), which were thus negatively impacted by the increase in current at 700 LMH. At effluent fluxes that allowed sufficient interaction of the antibiotics with the graphene-based sponge electrodes (i.e., 175 and 300 LMH), the obtained removal efficiencies of the target antibiotics at 144 A m^{-2} of anodic current were in the range from 79-97% (175 LMH) and 65-90% (300 LMH) (**Figure 1B**). Thus, it can be concluded that the lower removal of antibiotics at higher flowrates is a consequence of both mass transfer limitations (as observed in the OC for ERT and SMX, and to some degree TMP) and more intense formation of O_2 and H_2 bubbles (as observed during current application).

The bimolecular rate constants of the target antibiotics with ozone were in the order of 10^4-10^6 M^{-1} s^{-1} (**Table S3**) and indicate their moderate reactivity with ozone. In comparison, their bimolecular rate constants for the reaction with $^•OH$ were three orders of magnitude higher (10^9, **Table S3**). Cathodically formed H_2O_2 (i.e., up to 2 mg L^{-1} detected at 144 A m^{-2}) is activated to $^•OH$ at the N-active sites (Su et al., 2019), as well as by the anodically formed ozone. Also, $^•OH$ can also be formed at the BRGO anode by O_3 decomposition. Electrochemical generation of $^•OH$ via direct electrolysis of water, common for other anode materials (e.g., BDD), is unlikely to occur at the graphene-based sponge anode due to its high hydrophobicity, although it cannot be ruled out (Baptista-Pires et al., 2021). Nevertheless, given the much higher concentration of ozone (i.e., 0.25 mg L^{-1} at 144 A m^{-2}) compared with the $^•OH$ radical (i.e., 9.7×10^{-14} M at 144 A m^{-2}, **Table 2**), it is likely that both O_3 and $^•OH$ participated in the electrochemical degradation of the target antibiotics. It is important to note that the reported concentrations of $^•OH$ are conservative estimates, since the exact amount of $^•OH$ reacting with TA is unknown (Nayak and Chaplin, 2018). The role of $OH^•$ formed by the H_2O_2 activation at the NRGO cathode was also confirmed in the study of electrochemical transformation ERT . In addition, direct electrolysis of the adsorbed contaminants likely contributed to the degradation of the adsorbed and electrosorbed antibiotics, as was previously reported in the RGO-based sensing of organic pollutants (Bai et al., 2013; Qian et al., 2021). Demonstration of direct electrolysis mechanism at graphene-based sponges, e.g., via linear sweep voltammetry, is not possible due to the high capacitive current and oxygen evolution starting at potentials around 1.2-1.3 V/SHE. In addition, adsorption of antibiotics to the graphene-based sponges makes the elucidation of their oxidation mechanisms extremely difficult.
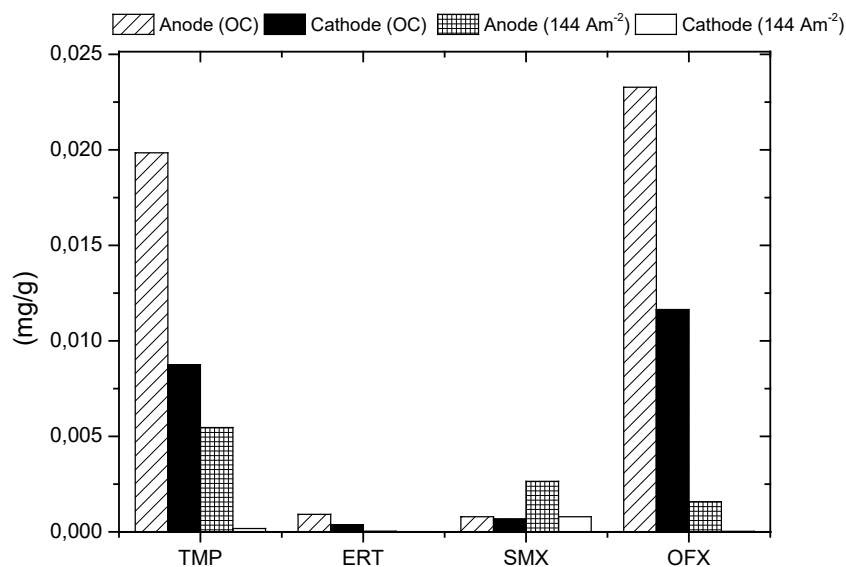
Figure 2. Measured amounts of the target antibiotics (mg) per gram of graphene sponges, extracted from the BRGO and NRGO sponges employed in the reactors operated in the OC and with application of 144 A m^{-2}, during 28 h run at 87.5 LMH; 10 mM phosphate buffer (pH 7), 0.2 µM as the initial concentration of antibiotics.

Electrochemical degradation of the adsorbed antibiotics was confirmed by the extraction of the target antibiotics from the BRGO and NRGO sponges employed in the OC only, and with the application of current (i.e., 144 A m^{-2}). Extraction of the antibiotics from the BRGO and NRGO sponges used in the OC was efficient for TMP and OFX that reacted with the RGO via π-π interactions, whereas more weekly adsorbing ERT and SMX could not be extracted using the employed protocol. The employed extraction protocol showed 57.7% and 56.5% of extraction recovery for TMP and OFX, yet <1% of ERT retained on the BRGO and NRGO sponges in the OC experiment could be recovered with methanol. Determination of the fraction of ERT adsorbed onto the graphene sponges would require further optimization of the extraction protocol and was out of scope of the present study; electrooxidation of ERT was confirmed in the study of its TPs, as explained further in the text. **Figure 2** summarizes the amounts of the antibiotics extracted from the BRGO and NRGO sponges used in the OC and with the application of 144 A m^{-2}. The extracted

concentrations of TMP and OFX were 4-fold and 15-fold higher, respectively, for the BRGO employed in the OC compared to the BRGO anodically polarized at 144 A m^{-2}. Similar results were obtained for the NRGO sponge, with 50-fold and 373-fold higher amounts of TMP and OFX, respectively, extracted from the NRGO sponge used in the OC, compared with the catholically polarized NRGO sponge. Thus, antibiotics and trace organic contaminants that are adsorbed onto the graphene-based sponge electrodes are also further electrochemically degraded.

To gain more insight into the impact of the anodic current, the reactor was operated in the OC during 48 h at low effluent flux (87.5 LMH) to allow the enrichment of the graphene sponges with the target antibiotics. The removal of SMX and OFX in the 48 h OC run remained unchanged (9% and 90-95%, respectively) confirming the low adsorption affinity of SMX and very strong π-π stacking of OFX at the graphene sponges. When the adsorption of organic contaminants is governed by their π-stacking with graphene-based materials, such is the case of OFX, it may proceed via multilayer adsorption and self-aggregation mechanism, which typically leads to high adsorption capacities (Tang et al., 2018). The removals of ERT and TMP were decreased from 80% (new sponges) to 28% and 39% after the 48 h OC run, respectively, indicating partial saturation of the sponges with these compounds (**Figure 3**). Application of 144 A m^{-2} of anodic current led to a gradual decrease in the effluent concentrations of SMX, TMP and ERT, for with complete removal (>90%) observed after approximately 25 bed volumes in the case of SMX and 50-70 bed volumes in the case of TMP and ERT. Thus, when the sponges were partially saturated with these contaminants, the system needed a longer time to reach a steady state than in the case of the unsaturated sponges. After switching off the current, effluent concentrations of SMX, TMP and ERT were gradually increased, evidencing the

enhancing impact of the current on the removal and electrochemical degradation of the target antibiotics. Moreover, effluent concentrations of the target antibiotics in the final OC run were all below the influent concentrations (C_0) in all samples, thus excluding their accumulation at the electrodes. The concentrations of ERT in the final OC were also below the concentrations measured in the initial OC_0 (**Figure 3**), suggesting the degradation of the adsorbed ERT and regeneration of the graphene-based sponge surface.
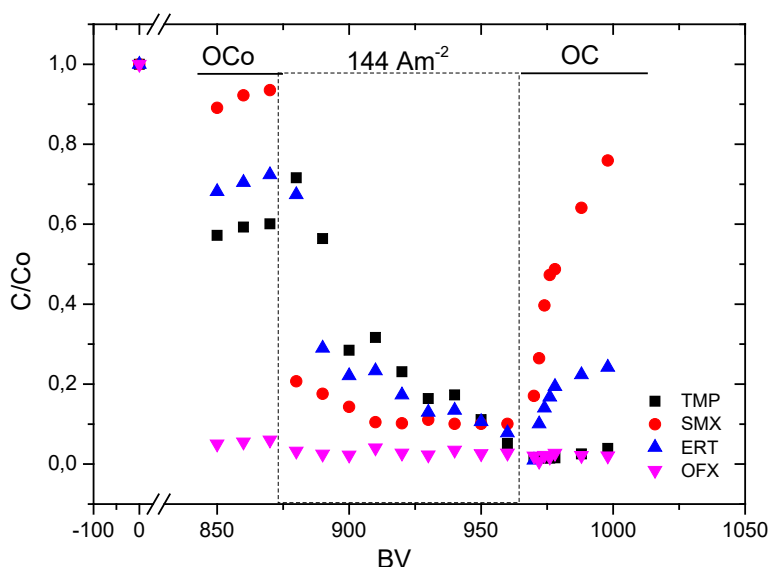
Figure 3. Concentrations (C) of the target antibiotic normalized to the initial value (C_0) for the experiments conducted with the initial open circuit (OC_0) run of 48 h, using 10 mM phosphate buffer, pH 7.

The E_{EO} values for the electrochemical removal of antibiotics at 144 A m^{-2} and 175 LMH of electrolyte flowrate when the sponges were partially saturated, were 10.8 (TMP), 10.2 (SMX), 9.8 (ERT), and 6.7 kWh m^{-3} (OFX). These values clearly indicate the importance of π-π interactions of the trace organic contaminants and their efficient interaction with the graphene sponges, with the strongest adsorbing OFX resulting in the lowest E_{EO} value. Similar results were obtained in our previous study, where triclosan had a significantly lower E_{EO} value (5.8 kWh m^{-3}) compared with the non-adsorbing iodinated contrast media diatrizoate and iopromide (11.2-15.1 kWh m^{-3}), and the negatively charged

diclofenac (12.9 kWh m^{-3}) (Baptista-Pires et al., 2021). Previously, E_{EO} for electrooxidation of using TiO$_2$ nanotube-SnO$_2$-Sb/polytetrafluoroethylene-PbO$_2$ anode was 5.4 kWh m^{-3}, however using a highly concentrated OFX solution and a high conductivity electrolyte (20 mg L^{-1}, 50 mM Na$_2$SO$_4$) (Xie et al., 2017). Anodic oxidation of TMP in the municipal sewage effluent required ~23 kWh m^{-3} for an order of removal using BDD anode (Moreira et al., 2016). Electrochemical degradation of tetracycline using a carbon nanotube (CNT) filter required only 0.084 kWh m^{-3} (10 mM Na$_2$SO$_4$, 200 µM initial concentration) due to its rapid adsorption onto the CNTs (Liu et al., 2015). Electrochemical oxidation of SMX using flow-through Magnéli phase reactive electrochemical membrane required only 0.27-0.33 kWh m^{-3}, although both the initial SMX concentration and supporting electrolyte conductivity were significantly higher than in our study (i.e., 100 µM SMX, 100 mM NaClO$_4$, pH 5.4) (Misal et al., 2020). Low conductivity of the supporting electrolyte significantly limits the electrocatalytic activity of the electrodes and ion transport towards the electrode surface due to the increased thickness of the double layer (Xie et al., 2017), as was also observed in our experiments with real tap water discussed further in the text. Thus, the comparison of the E_{EO} values obtained in different studies is complicated not only by the different reactor designs (e.g., flow-through vs flow-by mode, interelectrode distance), but also by the diverse operating conditions employed.

Electrochemical removal of antibiotics in tap water

When electrochemical system was operated with real tap water, the observed removals in the OC differed significantly from the data obtained for the phosphate buffer solution (**Table 1**). For example, the removal efficiency of TMP in the initial OC in phosphate buffer was 80%, whereas in tap water TMP did not adsorb onto the graphene sponge.

Also, ERT and OFX were adsorbed up to 50% and 41% in tap water, significantly lower compared with 81% and 90% in the OC performed in the phosphate buffer, respectively. Only in the case of SMX, the removal in the initial OC was similar, with around 12% adsorbed in tap water, compared to ~8% in the case of phosphate buffer. Decreased adsorption of ERT, TMP and OFX in tap water can be explained by its significantly lower conductivity (0.4-0.45 mS cm^{-1}) compared with the 10 mM phosphate buffer (1 mS cm^{-1}). By lowering the ionic strength, the thickness of the electric double layer at the surface of the graphene sponges is increased, which limits the electrostatic and ionic interaction between the target contaminants and the electrode surface(Liu et al., 2019; Wang et al., 2015). Lower ionic strength will also impact the surface interaction of both polar and nonpolar functional groups of organic molecules through decreased ion bridging and thus lowered adhesion of organic molecules to the graphene surface (Liu et al., 2019). Also, organic matter (i.e., 2 mg L^{-1}) and divalent cations such as Ca^{2+} and Mg^{2+} were present in the tap water (**Table S4**) and may have impacted the interaction of the target contaminants and the graphene sponge surface, e.g., through competitive electrosorption.

Table 1. Removal (%) of the target antibiotics in the open circuit (OC) and at the highest applied current in 10 mM phosphate buffer (PB, 144 A m^{-2}) and tap water (TW, 86 A m^{-2}), at 175 LMH.

	OC, 10 mM PB	OC, TW	144 A m^{-2}, 10 mM PB	86 A m^{-2}, TW
TMP	80±2.4	4.6±0.71	83±0.47	46±1
SMX	7.7±0.48	12±2	78.6±0.98	82±2
ERT	80.7±2.6	49.9±4	92.1±0.53	74.7±0.6
OFX	90.4±2.3	41.3±0.67	97.9±0.23	85±1

At 86 A m^{-2} of applied anodic current the ohmic-drop corrected anode potential was 4.75 V/SHE, somewhat higher than the value obtained for 10 mM phosphate buffer at 144 A m^{-2} (3.8 V/SHE). The effluent concentrations of the target antibiotics at 86 A m^{-2} in tap water were further lowered compared to the OC run, to reach the removal efficiencies of

85% (OFX), 82% (SMX), 74.7% (ERT) and 46% (TMP). Thus, the removal obtained at 86 A m^{-2} in tap water was lower compared with the experiments conducted in phosphate buffer as supporting electrolyte (**Table 1**). The amounts of the formed oxidant species were similar for the 10 mM phosphate buffer at 144 A m^{-2} and tap water at 86 A m^{-2} of applied current (**Table 2**). For example, the measured amounts of H_2O_2 were 2.5 and 2.1 mg L^{-1} in the tap water and 10 mM phosphate buffer, respectively. Although the measured concentrations of ozone and $^\bullet$OH were slightly higher for 10 mM phosphate buffer than for tap water, limited interaction of antibiotics with the graphene-based sponges in the lower ionic strength tap water was likely the main reason for their worsened electrochemical removal. The energy consumed by the system to achieve a 75%, 46%, 82% and 85 % removal of ERT, TMP, SMX and OFX, respectively, at the effluent flux of 175 LMH was 10.4 kWh m^{-3}.

Table 2. Oxidant concentrations determined in A-C ($^\bullet$OH, H_2O_2) and C-A (O_3) flow direction at 144 A m^{-2} and using 10 mM PB and TW, and flow rate of 175 LMH.

	10 mM PB	TW
O_3 (mg L^{-1})	0.25 ± 0.028	0.425 ± 0.1
H_2O_2 (mg L^{-1})	2.5 ± 0.0472	2.1 ± 0.0481
$^\bullet$OH (M)	$9.7 \times 10^{-14} \pm 7.7235 \times 10^{-17}$	$4.14 \times 10^{-14} \pm 1.3610^{-16}$

Elucidation of the transformation products of ERT

Electrochemical degradation of ERT yielded several TPs, out of which three could be identified with the employed analytical methodology. Namely, TP720 (molecular ion, [M+H]$^+$ 720.5) was formed by the demethylation of the desosamine moiety of ERT (**Figure S8**). Due the poor reactivity of the protonated dimethylamine group of ERT with ozone (Lee and Von Gunten, 2016), its demethylation was likely induced by the electrogenerated $^\bullet$OH. The same products was previously observed in O_3, O_3/UV and O_3/H_2O_2 oxidation of ERT(Luiz et al., 2010). Demethylation of the protomated -N$^+$(CH$_3$)$_2$

group stems from the attack of the OH• and abstraction of hydrogen at nitrogen and carbon atom(Das and von Sonntag, 1986). Further loss of the hydroxyl group from the desosamine moiety and oxidation of the hydroxyl group to keto group in the cladinose moiety yielded product TP702 ([M+H]$^+$ 702.4) presented in **Figure S9**. Oxidative cleavage of the C-O bond and loss of the cladinose moiety yielded the product TP576 ([M+H]$^+$ 576.4, **Figure S10**). These products have been previously identified in the ozonation and OH•- based oxidation processes (Kim et al., 2020; Li et al., 2017; Luiz et al., 2010; Michael-Kordatou et al., 2015). According to these studies, when reacting with O$_3$ and •OH, the major structural alterations in the ERT molecule occur at the macrolide and cladinose moieties, as observed in our study. The identified products were detected in the samples taken after both BRGO anode and NRGO cathode. The group responsible for the antibiotic activity in the macrolide antibiotics is the dimethylamine group of the desosamine moiety, which mediates the hydrogen bonding of ERT and peptydyl transferase cavity of bacterial ribosomes (Moreira et al., 2016). Thus, the identified products TP720 and TP702 that uderwent cleavage of the methyl group in this moiety may not pose a threat, whereas TP576 will likely have preserved the antibiotic activity (**Figuere 4**). Nevertheless, the experiments aiming at the identification of TPs of ERT were conducted at high initial ERT concentration (20 μM), and the electrochemical degradation of ERT and other model antibiotics at the developed graphene sponge electrodes should be further studied at environmentally relevant concentrations. In addition, three more peaks were assigned to specific molecular ions but the mass spectra obtained did not allow their identification, namely TP734 ([M+H]$^+$ 734.4), TP526 ([M+H]$^+$ 526.4), and 540 ([M+H]$^+$ 540.4) and 558 ([M+H]$^+$ 558.4) (**Figure S11-14**). Structural elucidation of these TPs requires high resolution mass spectrometry and will be the subject of our future studies.
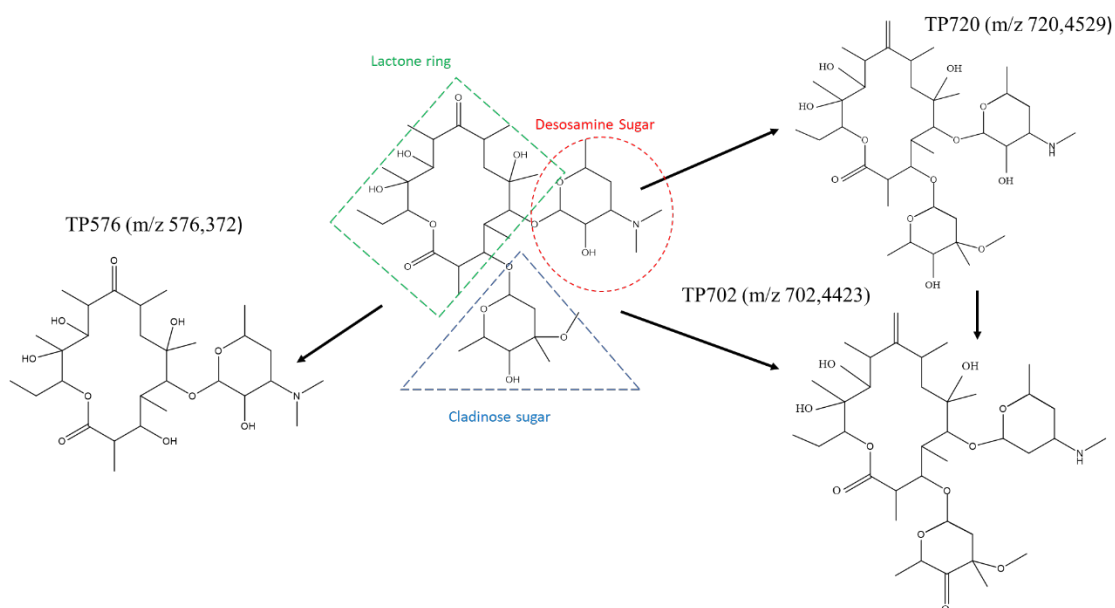
Figure 4. Transformation products (TPs) of ERT tentatively identified using CID MS^2 experiments in (+) ESI mode and mass spectral comparison with the parent compound.

Conclusions

Graphene-based sponge electrodes doped with boron (anode) and nitrogen (cathode) were employed for electrochemical removal of antibiotics from a low conductivity supporting electrolyte (i.e., 1 mS cm^{-1}). The removal of strongly adsorbing OFX rich in aromatic rings was dominated by the π-π interactions and was less limited by the mass transfer. At the highest applied effluent flux of 700 LMH, higher currents had a detrimental impact on the removal of TMP, OFX and ERT due to the more intense production of oxygen and hydrogen bubbles, and decreased interaction of antibiotics with the graphene sponges. This could be resolved by improving the evacuation of gas bubbles, e.g., by using thinner graphene sponge electrodes and is currently under investigation in our group. In the case of negatively charged SMX, increase in current improved its removal even at high applied flowrates, likely to to its enhanced electrosorption onto the positively charged BRGO anode. Electrochemical degradation of the adsorbed target antibiotics was confirmed by their extraction from the sponges employed in the OC and with the application of current,

with 50-373-fold lower amounts of the strongly adsorbing antibotics (i.e., TMP and OFX) obtained in the latter case. Elucidation of the products formed in electrochemical degradation of ERT confirmed the participation of $^{\bullet}$OH in its oxidation, e.g., through the demethylation of the desosamine moiety.

When using real tap water, electrochemical removal of target antibiotics was lowered from 79-98% in 10 mM phosphate buffer to 46-85% in tap water. Similar steady state concentrations of major oxidants were measured for 10 mM phosphate buffer (144 A m^{-2}, anode corrected potential 3.8 V/SHE) and tap water (86 A m^{-2}, anode corrected potential 4.75V/SHE). Thus, the detrimental effect of the lower ionic strength of the tap water was assigned to the lowered interaction of antibiotics with the graphene sponge surface due to the increased thickness of the double layer at the electrode surface, as also evidenced by the significantly lower removals in the OC run in tap water. Although the removal of some antibiotics was incomplete in tap water (e.g., trimethoprim, 46% removal), reactor performance can be improved by providing a higher electrode surface area. The estimated cost of the developed graphene sponge is less than €50 per m^2 of the material projected surface area (Baptista-Pires et al., 2021; Norra et al., 2022). Given that the anodically polarized graphene sponge is electrochemically inert towards chloride, the developed material can enable a safe application of electrochemical process for the removal of antibiotics and other organic contaminants, without increasing the toxicity of the treated water.

Supplementary Material

Scheme of the of the one-pass flow-through reactor reactor. The optimized compound-dependent MS-parameters. MS2 mass spectra, total and extracted ion chromatograms of the TPs of ERT. Graphene sponge materials characterization (SEM). Chemical structures

and physico-chemical properties of target contaminants and Bimolecular rate constants.

Ozone and peroxide formation and electrochemical degradation of pollutants. Methanol

extraction of the antibiotics. Tap water characteristics and electrochemical degradation of

pollutants in tap water.

Acknowledgments

References

Bai, S., Shen, X., Zhu, G., Yuan, A., Zhang, J., Ji, Z., Qiu, D., 2013. The influence of wrinkling in reduced graphene oxide on their adsorption and catalytic properties. Carbon 60, 157–168. doi: 10.1016/j.carbon.2013.04.009

Baptista-Pires, L., Norra, G.F., Radjenovic, J., 2021. Graphene-based sponges for electrochemical degradation of persistent organic contaminants. Water Res. 203, 117492. doi: 10.1016/j.watres.2021.117492

Ben, Y., Hu, M., Zhang, X., Wu, S., Wong, M.H., Wang, M., Andrews, C.B., Zheng, C., 2020. Efficient detection and assessment of human exposure to trace antibiotic residues in drinking water. Water Res. 175, 115699. doi: 10.1016/j.watres.2020.115699

Boy-Roura, M., Mas-Pla, J., Petrovic, M., Gros, M., Soler, D., Brusi, D., Menció, A., 2018. Towards the understanding of antibiotic occurrence and transport in groundwater: Findings from the Baix Fluvià alluvial aquifer (NE Catalonia, Spain). Sci. Total Environ. 612, 1387–1406. doi: 10.1016/j.scitotenv.2017.09.012

Bryan-Wilson, J., 2016. No time to wait. Artforum Int. 54, 113–114.

Cacace, D., Fatta-Kassinos, D., Manaia, C.M., Cytryn, E., Kreuzinger, N., Rizzo, L., Karaolia, P., Schwartz, T., Alexander, J., Merlin, C., Garelick, H., Schmitt, H., de Vries, D., Schwermer, C.U., Meric, S., Ozkal, C.B., Pons, M.N., Kneis, D., Berendonk, T.U., 2019. Antibiotic resistance genes in treated wastewater and in the receiving water bodies: A pan-European survey of urban settings. Water Res. 162, 320–330. doi: 10.1016/j.watres.2019.06.039

Carrales-Alvarado, D.H., Rodríguez-Ramos, I., Leyva-Ramos, R., Mendoza-Mendoza, E., Villela-Martínez, D.E., 2020. Effect of surface area and physical–chemical properties of graphite and graphene-based materials on their adsorption capacity towards metronidazole and trimethoprim antibiotics in aqueous solution. Chem. Eng. J. 402, 126155.doi: /10.1016/j.cej.2020.126155

Carvalho, I.T., Santos, L., 2019. Antibiotics in the aquatic environments: A review of the European scenario. Environ. Int. 94, 736–757. doi: 10.1016/j.envint.2016.06.025

Chaplin, B.P., 2019. The Prospect of Electrochemical Technologies Advancing Worldwide Water Treatment. Acc. Chem. Res. 52, 596–604. doi: 10.1021/acs.accounts.8b00611

Chaplin, B.P., 2014. Critical review of electrochemical advanced oxidation processes for water treatment applications. Environ. Sci. Process. Impacts 16, 1182–1203. doi: 10.1039/c3em00679d

Das, S., von Sonntag, C., 1986. The Oxidation of Trimethylamine by OH Radicals in Aqueous Solution, as Studied by Pulse Radiolysis, ESR, and Product Analysis. The Reactions of the Alkylamine Radical Cation, the Aminoalkyl Radical, and the Protonated Aminoalkyl Radical. Zeitschrift fur Naturforsch. - Sect. B J. Chem. Sci. 41, 505–513. doi: 10.1515/znb-1986-0418

Ehtesabi, H., Bagheri, Z., Yaghoubi-Avini, M., 2019. Application of three-dimensional graphene hydrogels for removal of ofloxacin from aqueous solutions. Environ. Nanotechnol. Monit. Manag. 12, 100274. doi: 10.1016/j.enmm.2019.100274

Gu, X., Zhai, H., Cheng, S., 2021. Fate of antibiotics and antibiotic resistance genes in home water purification systems. Water Res. 190, 116762. doi: 10.1016/j.watres.2020.116762

Jing, Y., Chaplin, B.P., 2017. Mechanistic study of the validity of using hydroxyl radical probes to characterize electrochemical advanced oxidation processes. doi: 10.1021/acs.est.6b05513

Kaur, R., Kushwaha, J.P., Singh, N., 2019. Electro-catalytic oxidation of ofloxacin antibiotic in continuous reactor: evaluation, transformation products and pathway. J. Electrochem. Soc. 166, H250–H261. doi: 10.1149/2.1281906jes

Khan, S., Knapp, C.W., Beattie, T.K., 2016. Antibiotic resistant bacteria found in municipal drinking water. Environ. Process. 3, 541–552. doi: 10.1007/s40710-016-0149-z

Kim, T.K., Kim, T., Cha, Y., Zoh, K.D., 2020. Energy-efficient erythromycin degradation using UV-LED (275 nm)/chlorine process: radical contribution, transformation products, and toxicity evaluation. Water Res. 185, 116159. doi: 10.1016/j.watres.2020.116159

Lee, Y., Von Gunten, U., 2016. Advances in predicting organic contaminant abatement during ozonation of municipal wastewater effluent: Reaction kinetics, transformation products, and changes of biological effects. Environ. Sci. Water Res. Technol. 2, 421–442. doi: 10.1039/c6ew00025h

Li, M., Yang, X., Wang, D.S., Yuan, J., 2017. Enhanced oxidation of erythromycin by persulfate activated iron powder–H_2O_2 system: role of the surface Fe species and synergistic effect of hydroxyl and sulfate radicals. Chem. Eng. J. doi: 10.1016/j.cej.2016.12.126

Liang, S., Lin, H., Yan, X., Huang, Q., 2018. Electro-oxidation of tetracycline by a Magnéli phase Ti_4O_7 porous anode: Kinetics, products, and toxicity. Chem. Eng. J. 332, 628–636. doi: 10.1016/j.cej.2017.09.109

Liu, Y., Liu, H., Zhou, Z., Wang, T., Ong, C.N., Vecitis, C.D., 2015. Degradation of the common aqueous antibiotic tetracycline using a carbon nanotube electrochemical

filter. Environ. Sci. Technol. 49, 7974–7980. doi: 10.1021/acs.est.5b00870

Liu, Z., Rios-Carvajal, T., Andersson, M.P., Ceccato, M., Stipp, S.L.S., Hassenkam, T., 2019. Ion effects on molecular interaction between graphene oxide and organic molecules. Environ. Sci. Nano 6, 2281–2291. doi: 10.1039/c9en00274j

Luiz, D.B., Genena, A.K., Virmond, E., José, H.J., Moreira, R.F.P.M., Gebhardt, W., Schröder, H.F., 2010. Identification of degradation products of erythromycin A arising from ozone and advanced oxidation process treatment. Water Environ. Res. 82, 797–805. doi. 10.2175/106143010x12609736966928

Ma, Y., Li, M., Wu, M., Li, Z., Liu, X., 2015. Occurrences and regional distributions of 20 antibiotics in water bodies during groundwater recharge. Sci. Total Environ. 518–519, 498–506. doi: 10.1016/j.scitotenv.2015.02.100

Michael-Kordatou, I., Iacovou, M., Frontistis, Z., Hapeshi, E., Dionysiou, D.D., Fatta-Kassinos, D., 2015. Erythromycin oxidation and ERY-resistant Escherichia coli inactivation in urban wastewater by sulfate radical-based oxidation process under UV-C irradiation. Water Res. 85, 346–358. doi: 10.1016/j.watres.2015.08.050

Misal, S.N., Lin, M.H., Mehraeen, S., Chaplin, B.P., 2020. Modeling electrochemical oxidation and reduction of sulfamethoxazole using electrocatalytic reactive electrochemical membranes. J. Hazard. Mater. 384, 121420. doi: 10.1016/j.jhazmat.2019.121420

Mordačíková, E., Vojs, M., Grabicová, K., Marton, M., Michniak, P., Řeháček, V., Bořík, A., Grabic, R., Bruncko, J., Mackuľak, T., Vojs Staňová, A., 2020. Influence of boron doped diamond electrodes properties on the elimination of selected pharmaceuticals from wastewater. J. Electroanal. Chem. 862. doi: 10.1016/j.jelechem.2020.114007

Moreira, F.C., Soler, J., Alpendurada, M.F., Boaventura, R.A.R., Brillas, E., Vilar, V.J.P., 2016. Tertiary treatment of a municipal wastewater toward pharmaceuticals removal by chemical and electrochemical advanced oxidation processes. Water Res. 105, 251–263. doi: 10.1016/j.watres.2016.08.036

Nayak, S., Chaplin, B.P., 2018. Fabrication and characterization of porous, conductive, monolithic Ti_4O_7 electrodes. Electrochim. Acta 263, 299–310. doi: 10.1016/j.electacta.2018.01.034

Norra, G.F., Baptista-Pires, L., Cuervo Lumbaque, E., Borrego, C.M., Radjenović, J., 2022. Chlorine-free electrochemical disinfection using graphene sponge electrodes. Chem. Eng. J. 430, 132772. doi: 10.1016/j.cej.2021.132772

O'Connor, S., Aga, D.S., 2007. Analysis of tetracycline antibiotics in soil: Advances in extraction, clean-up, and quantification. Trends Anal. Chem. 26, 456–465. doi: 10.1016/j.trac.2007.02.007

Pruden, A., Arabi, M., Storteboom, H.N., 2012. Correlation between upstream human activities and riverine antibiotic resistance genes. Environ. Sci. Technol. 46, 11541–11549. doi: 10.1021/es302657r

Qian, L., Thiruppathi, A.R., Van Der Zalm, J., Chen, A., 2021. Graphene oxide-based nanomaterials for the electrochemical sensing of isoniazid. ACS Appl. Nano Mater. 4, 3696–3706. doi: 10.1021/acsanm.1c00178

Radjenovic, J., Bagastyo, A., Rozendal, R.A., Mu, Y., Keller, J., Rabaey, K., 2011. Electrochemical oxidation of trace organic contaminants in reverse osmosis concentrate using RuO_2/IrO_2-coated titanium anodes. Water Res. 45, 1579–1586. doi: 10.1016/j.watres.2010.11.035

Radjenovic, J., Sedlak, D.L., 2015. Challenges and Opportunities for Electrochemical Processes as Next-Generation Technologies for the Treatment of Contaminated Water. Environ. Sci. Technol. 49, 11292–11302. doi: 10.1021/acs.est.5b02414

Ramezanzadeh, B., Haeri, Z., Ramezanzadeh, M., 2016. A facile route of making silica nanoparticles-covered graphene oxide nanohybrids (SiO_2-GO); fabrication of SiO_2-GO/epoxy composite coating with superior barrier and corrosion protection performance. Chem. Eng. J. 303, 511–528. doi: 10.1016/j.cej.2016.06.028

Sabri, N.A., van Holst, S., Schmitt, H., van der Zaan, B.M., Gerritsen, H.W., Rijnaarts, H.H.M., Langenhoff, A.A.M., 2020. Fate of antibiotics and antibiotic resistance genes during conventional and additional treatment technologies in wastewater treatment plants. Sci. Total Environ. 741, 140199. doi: 10.1016/j.scitotenv.2020.140199

Shemella, P., Nayak, S.K., 2009. Electronic structure and band-gap modulation of graphene via substrate surface chemistry. Appl. Phys. Lett. 94, 1–3. doi: 10.1063/1.3070238

Su, H.C., Liu, Y.S., Pan, C.G., Chen, J., He, L.Y., Ying, G.G., 2018. Persistence of antibiotic resistance genes and bacterial community changes in drinking water treatment system: From drinking water source to tap water. Sci. Total Environ. 616–617, 453–461. doi: 10.1016/j.scitotenv.2017.10.318

Su, P., Zhou, M., Lu, X., Yang, W., Ren, G., Cai, J., 2019. Electrochemical catalytic mechanism of N-doped graphene for enhanced H_2O_2 yield and in-situ degradation of organic pollutant. Appl. Catal. B Environ. 245, 583–595. doi: 10.1016/j.apcatb.2018.12.075

Tang, H., Zhao, Y., Shan, S., Yang, X., Liu, D., Cui, F., Xing, B., 2018. Theoretical insight into the adsorption of aromatic compounds on graphene oxide. Environ. Sci. Nano 5, 2357–2367. doi: 10.1039/c8en00384j

Wang, F., Ma, S., Si, Y., Dong, L., Wang, X., Yao, J., Chen, H., Yi, Z., Yao, W., Xing, B., 2017. Interaction mechanisms of antibiotic sulfamethoxazole with various graphene-based materials and multiwall carbon nanotubes and the effect of humic acid in water. Carbon 114, 671–678. doi: 10.1016/j.carbon.2016.12.080

Wang, F., Shih, K.M., Li, X.Y., 2015. The partition behavior of perfluorooctanesulfonate (PFOS) and perfluorooctanesulfonamide (FOSA) on microplastics. Chemosphere 119, 841–847. doi: 10.1016/j.chemosphere.2014.08.047

Watkinson, A.J., Murby, E.J., Kolpin, D.W., Costanzo, S.D., 2009. The occurrence of antibiotics in an urban watershed: From wastewater to drinking water. Sci. Total Environ. 407, 2711–2723. doi: 10.1016/j.scitotenv.2008.11.059

Xie, R., Meng, X., Sun, P., Niu, J., Jiang, W., Bottomley, L., Li, D., Chen, Y., Crittenden, J., 2017. Electrochemical oxidation of ofloxacin using a TiO_2-based SnO_2-Sb/polytetrafluoroethylene resin-PbO_2 electrode: Reaction kinetics and mass

transfer impact. Appl. Catal. B Environ. 203, 515–525. doi: 10.1016/j.apcatb.2016.10.057

Yang, J., Wang, H., Roberts, D.J., Du, H.N., Yu, X.F., Zhu, N.Z., Meng, X.Z., 2020. Persistence of antibiotic resistance genes from river water to tap water in the Yangtze River Delta. Sci. Total Environ. 742, 140592. doi: 10.1016/j.scitotenv.2020.140592

Zhao, G., Zhu, H., 2020. Cation–π interactions in graphene-containing systems for water treatment and beyond. Adv. Mater. 32, 1–22. doi: 10.1002/adma.201905756

Supplementary Material

Electrochemical degradation of antibiotics using flow-through graphene sponge electrodes

Natalia Ormeno-Cano[a,b], Jelena Radjenovic [a,c]*

[a]Catalan Institute for Water Research (ICRA- CERCA), c/Emili Grahit, 101, 17003 Girona, Spain

[b]University of Girona, Girona, Spain

[c]Catalan Institution for Research and Advanced Studies (ICREA), Passeig Lluís Companys 23, 08010 Barcelona, Spain

* Corresponding author:

Jelena Radjenovic, Catalan Institute for Water Research (ICRA), Scientific and Technological Park of the University of Girona, 17003 Girona, Spain

Phone: + 34 972 18 33 80; Fax: +34 972 18 32 48; E-mail: jradjenovic@icra.cat

31

Text S1. Characterization of the synthesized graphene-based sponges.

The characterization of the BRGO and NRGO sponges is reported in detail in our previous work [1,2]. Below is the summary of the main results.

Scanning electron microscopy (SEM) was performed using a FEI Quanta FEG (pressure: 70Pa; HV: 20kV; and spot: four). Dispersive spectrometer Jobin-Yvon LabRam HR 800, coupled to an optical microscope Olympus BXFM was used for Raman characterization. The CCD detector was cooled at -70OCVand a 532 nm laser line was used with a dispersive grating of 600 lines/mm and a laser power at sample of 0.5 mW.

The X-ray photoelectron spectroscopy (XPS) measurements were done with a Phoibos 150 analyzer (SPECS GmbH, Berlin, Germany) in ultra-high vacuum conditions (base pressure 1-10 mbar) with a monochromatic aluminium Kalpha x-ray source (1486.74 eV). The energy resolution as measured by the FWHM of the Ag 3d5/2 peak for a sputtered silver foil was 0.58 eV. The XPS analyses revealed a C/O atomic ratio of 1.7, 3.5 and 3.6 for GO, BRGO and NRGO, demonstrating an efficient hydrothermal reduction of GO. The atomic content of the GO precursor solution and synthesized graphene-based sponges was: 62.6% C, 36.9% O, 0.9% N for GO, 72.1% C, 19.9% O, 7.9% N for NRGO, and 75.6% C, 21.8% O, 1.2% N and 1.3% B for BRGO.Zeta potential of BRGO and NRGO was measured using Zetasizer Nano ZS (Malvern Panalytical Ltd) operating with a 633 nm laser and using an aqueous solution at pH 7. The zeta potentials of the BRGO and NRGO sponges were –36.2 mV and –13.3 mV, respectively.

Dispersive spectrometer Jobin-Yvon LabRam HR 800, coupled to an optical microscope Olympus BXFM was used for Raman characterization. The CCD detector was cooled at -70^{OCV} and a 532 nm laser line was used with a dispersive grating of 600 lines/mm and a laser power at sample of 0.5 mW. The Id/Ig ratios were calculated analyzing three different spots/areas per sample. The level of defects was calculated by measuring the intensity ratio of D peak at 1347 cm^{-1} (Id) and a G peak at 1581 cm^{-1} (Ig) obtained using Raman spectroscopy The higher the Id/Ig ratio is, the higher is the content of the graphene defects. The measured Id/Ig ratios were 1.07 for GO, 1.18 for BRGO and 1.21 for NRGO.

X-ray diffraction (XRD) analysis was performed with a X'pert multipurpose diffractometer using a Cu Kα radiation (l = 1.540 Å), at room temperature. It was equipped with a vertical θ–θ goniometer (240 mm radius) with fixed sample stages that do not rotate around the Ω axis as in the case of Ω–2θ diffractometers. An X'Celerator detector was utilized, which is an ultrafast X-ray detector based on real-time multiple strip technology. The diffraction pattern was recorded with a step size of 0.03°C and a time per step of 1,000 seconds, between 4°C and 30ºC. The XRD analysis showed a decrease in the interlayer spacing from 8.1 Å for GO to ≈ 3.5 Å for BRGO and NRGO, due to the removal of the oxygen functional groups from the basal plane.

The measurements of the contact angle of the synthesized graphene-based sponges were performed using EasyDrop Contact Angle Measuring Instrument by KRUSS GmbH in three different layers (one outer and two inner surfaces). The cross-plane electrical resistances of the graphene-based sponges were determined in a 0.5x0.5x0.5cm cube (x,y,z directions) between the two geometrically opposite faces. The contact angles determined for BRGO and NRGO were 139.67º±4.50º and 137.67º±7.50º, respectively, demonstrating a high degree of hydrophobicity of the sponges, similar to the previously

reported values. [3]
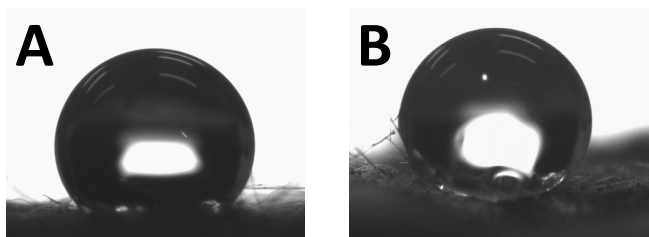
The Brunauer–Emmett–Teller (BET) specific surface areas were determined by N_2 adsorption-desorption at 77 K in (ASAP 2420, Micromeritics). The BET surface areas were 0.81 m^2 g^{-1} for the mineral wool template, 1.39 m^2 g^{-1} for the BRGO, and 1.44 m^2 g^{-1} for NRGO. The adsorption average pore width (4V/A by BET) was 80.1650 Å for BRGO and 64.0114 Å for NRGO, implying that the surface of the graphene sponges was mainly mesoporous.

Text S2. Calculation of the ohmic drop.

The ohmic drop was calculated from the Ohmic internal resistance obtained in the electrochemical impedance spectroscopy (EIS) experiments of the BRGO(A)-NRGO(C) system. Determination of ohmic drop allowed to calculate the ohmic-drop corrected anode potentials and allow better comparison of electrochemical system operating in 10 mM phosphate buffer and tap water, as the latter one will yield much higher ohmic resistance (due to lower electric conductivity of tap water) compared with the buffer solution. The Nyquist plots of the BRGO(A)-NRGO(C) system for real tap water (0.4-0.5 mS cm^{-1}) and 10 mM phosphate buffer (PB) (1 mS cm^{-1}) are shown in **Figure S4.**
In the circuit the ohmic internal resistance (R1) is connected in series with the capacitance (C2) and the charge transfer resistance R2 of the graphene sponge that are connected in parallel to each other. A constant phase element (Q3), representing the double layer capacitance, which occurs at the interface between the material and the electrolytes due to charge separation, is connected in parallel with a charge separation resistance R3, and Q4 that represents the ideal polarizable capacitance which would give rise to a straight line parallel to the imaginary axis. The obtained R1 was 10.8 Ω for 10 mM phosphate buffer and 27 Ω for tap water, thus resulting in the ohmic drop corrected potential of 3.80 V for 144 Am^{-2} of the applied anodic current in 10 mM phosphate buffer, and 4.75 V for 86 $Am^{-2}V$ of the applied anodic current in tap water, respectively. The ohmic drop-corrected anode potential (E_{corr}, V) was calculated according to the following equation:

$$E_{corr} = E_{rec} - (I \times R1) \qquad\qquad \text{(eq. S1)}$$

where I is the applied anodic current (A), $R1$ is the uncompensated resistance (Ω) and E_{rec} is the anode potential recorded in the chronopotentiometric experiments (V).

Text S3. Analysis of target antibiotics.

Sulfamethoxazole (SMX), ofloxacin (OFX), erythromycin (ERT), and trimethoprim (TMP) were analysed in electrospray (ESI) positive mode using an Acquity ultraperformance liquid chromatography (UPLC) HSS T3 column (2.1×50 mm, 1.8 µm, Waters) run at 30°C. The eluents employed were acetonitrile with 0.1% formic acid (eluent A), and milli-Q (LC-MS grade) water with 0.1% formic acid (eluent B) at a flow rate of 0.5 mL min^{-1}. The gradient was started at 2% of eluent A that was increased to 70% A by 4 min, further increased to 95% A by 5 min and it was kept constant by 5.5 min. Then, it was returned to the initial conditions of 2% A by 6 min further kept constant for 1 min. The total run time was 7 min. The target antibiotics were analysed in a multiple reaction monitoring (MRM). The settings for the compound-dependent parameters of each transition are summarized in **Table S1**. The source-dependent parameters were as follows: curtain gas (CUR), 30 V; nitrogen collision gas (CAD), medium; source temperature (TEM), 650°C; ion source gases GS1, 60 V and GS2, 50 V; ion spray voltage, 5500V, and entrance potential (EP), 10V.

Text S4. Current efficiencies (CE, %) for the electrogeneration of oxidant species were calculated from the formula (eq. S2):

$$\boldsymbol{CE}\ (\%) = \mathbf{100} * \boldsymbol{n} * \boldsymbol{F} * \boldsymbol{q} * \frac{c_t}{I} \qquad\qquad \textbf{(eq. S2)}$$

where n is the number of electrons required for production of specific oxidant (O_3, H_2O_2, $^{\bullet}OH$), F is the Faraday constant (96487 C mol^{-1}), q is the applied flowrate (L s^{-1}), I is the applied current (A) and C_t the measured molar concentration of a given oxidant species in the effluent.

Table S1. The optimized compound-dependent MS parameters: declustering potential (DP), collision energy (CE), and cell exit potential (CXP), for each compound and each transition of the negative and positive mode.

Target analyte	Q1 Mass (Da)	Q3 Mass (Da)	DP	CE	CXP
TMP	291.02	230.2	91	33	12
	291.021	261.1	91	35	10
SMX	253.992	156.1	81	23	12
	253.992	92.0	81	37	12
ERT	734.3	576.4	116	27	22
	734.3	158.1	116	39	14
OFX	362.038	318.3	86	27	12
	362.038	261.0	86	39	12

Table S2. Chemical structures and physico-chemical properties of target contaminants; molecular weight (MW), pKa, octanol-water distribution coefficient calculated based on chemical structure at pH 7.4 (ACD/logD), and polar surface area. Calculated ACD/logD values and polar surface areas were collected from Chemspider.com database.
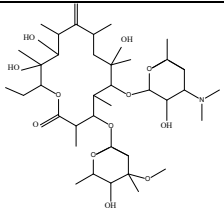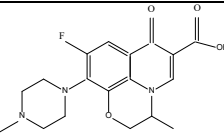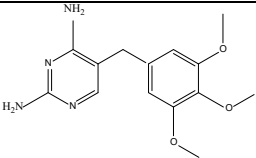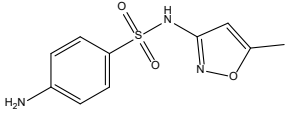
Organic compound (MW, g/mol)	Chemical structure	pKa	ACD/LogD[4]	Polar surface area (Å^2)[1]
Erythromycin (ERT) 733.93 g/mol		8.92[2]	1.69	194
Ofloxacin (OFX) 361.37 g/mol $C_{18}H_{20}FN_3O_4$		pK_{a1} = 5.97 pK_{a2} = 9.28 [5]	-2.08	73
Trimethoprim (TMP) 290.1 g/mol $C_{14}H_{18}N_4O_3$		pK_{a1} =3.2[6] pK_{a2} =7.1	-1.15	99
Sulfamethoxazole (SMX) 253.28 g/mol $C_{10}H_{11}N_3O_3S$		pK_{a1} =1.4[7] pK_{a1} =5.8	-0.56	107

Table S3. Reported bimolecular rate constants of target antibiotics with ozone (k_{O3}) and hydroxyl radicals (k_{OH}, $M^{-1} s^{-1}$).

Compound	k_{O3} ($M^{-1} s^{-1}$)	k_{OH} ($M^{-1} s^{-1}$)
Erythromycin (ERT) $C_{37}H_{67}NO_{13}$	$6.93.10^4$ [8]	5×10^9 [9]
Ofloxacin (OFX) $C_{18}H_{20}FN_3O_4$	2.0×10^6 [10]	4.2×10^9 [10]
Trimethoprim (TMP) $C_{14}H_{18}N_4O_3$	2.7×10^5	6.9×10^9 [11]
Sulfamethoxazole (SMX) $C_{10}H_{11}N_3O_3S$	5.5×10^5	5.5×10^9 [12]

Table S4 Tap water characteristics.

Conductivity (mS cm^{-1})	450
Total alkalinity (T_{AC}) mg L^{-1} CaCO$_3$	130.1
Cl$^-$, mg L^{-1}	21.4
SO$_4^{2-}$, mg L^{-1}	13.4
Na$^+$, mg L^{-1}	13.8
Mg^{2+}, mg L^{-1}	9.2
Ca^{2+}, mg L^{-1}	51.2
Total organic carbon (TOC), mg L^{-1}	2.1
pH	7.3

Table S5. Current efficiency (%) calculated for the formed oxidant species determined in A-C ($^{\bullet}$OH, H_2O_2) and C-A (O_3) flow direction at 144 A m^{-2} and using 10 mM phosphate buffer (PB) and tap water (TW), and flow rate of 175 LMH. It should be noted that the calculated current efficiencies for H_2O_2 production are underestimated values due to the in situ activation of H_2O_2 to $^{\bullet}$OH at the N-active sites of the NRGO cathode.

Current efficiency (%)	10 mM PB	TW
O_3	0.13	0.23
H_2O_2	0.47	0.4
$^{\bullet}$OH	$3.12*10^{-10}$	$1.33*10^{-10}$

Table S6. Recorded total cell potentials (Etot, V) for the four studied flow rates (87.5, 175, 300 and 700 LMH) at the different current applied (29, 86, and 144 Am^{-2}) in 10 mM of phosphate buffer and tap water.

	Etot (V), 10 mM phosphate buffer (PB)			
	87.5 LMH	**175 LMH**	**300 LMH**	**700 LMH**
29 Am^{-2}	5.4	6.4	6.5	6.4
86 Am^{-2}	6.1	11.3	11.1	14.2
144 Am^{-2}	8.1	14.9	14.6	20.6
	Etot (V), tap water (TW)			
	175 LMH			
86 Am^{-2}	24.8 V			

1)

2) Squeezing of mineral wool in GO-based precursor solution until completely soaked.

3) Soaked mineral wool is rolled up and placed in a hydrothermal reactor.

4) Hydrothermal tretment: 180ºC, 12h.

4,7 cm
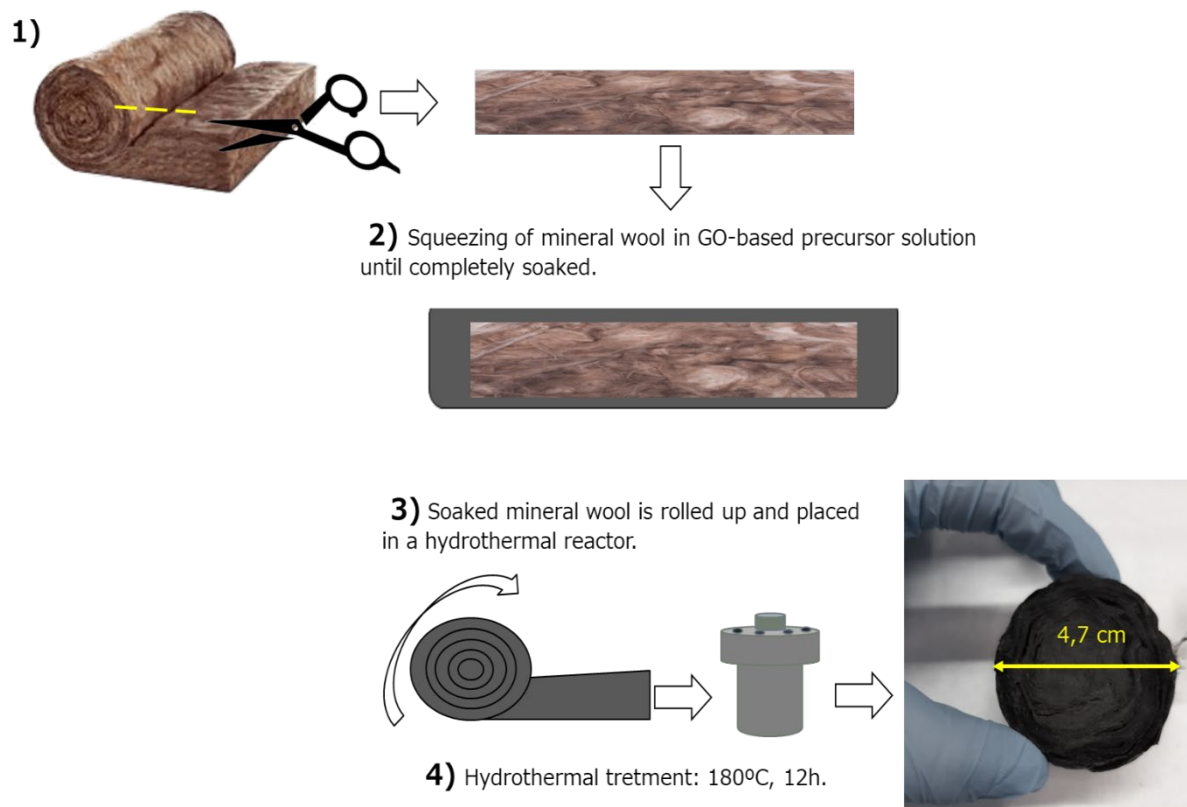
Figure S1. Schematic illustration of the synthesis methodology for BRGO and NRGO sponges.
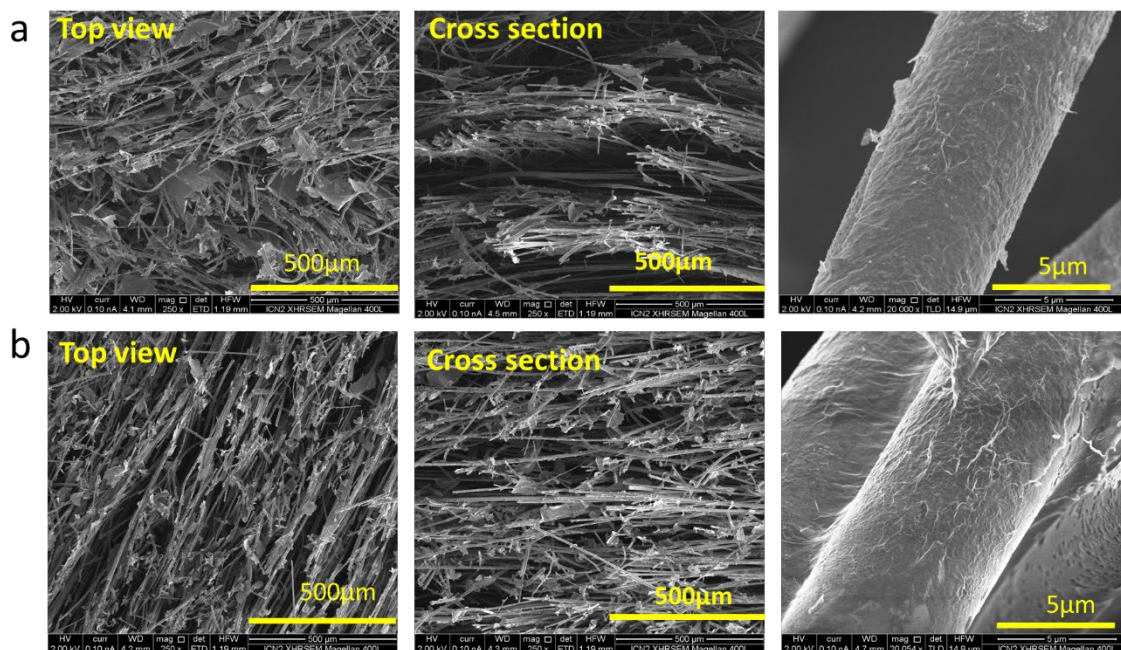
Figure S2. Scanning electron microscopy (SEM) images of **a)** BRGO, and **b)** NRGO.
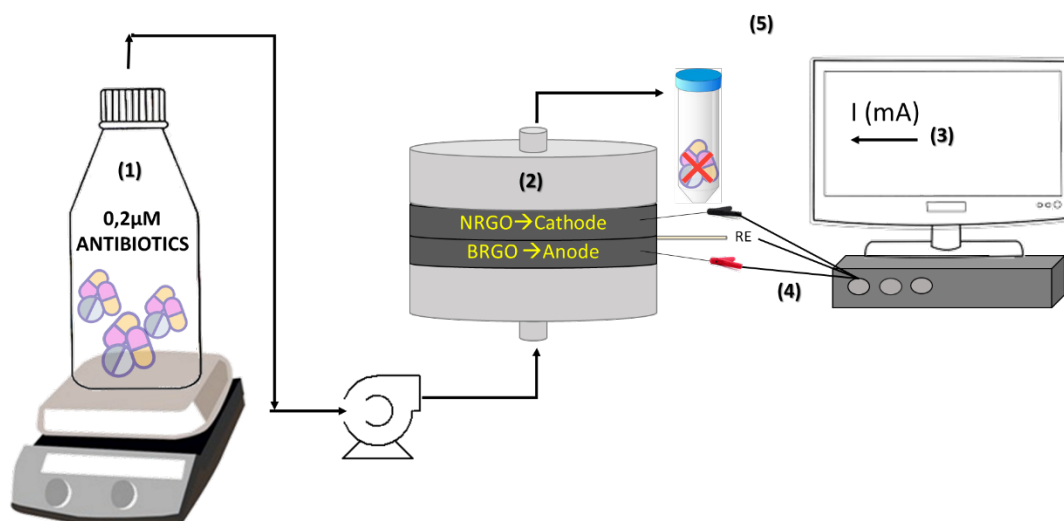
Figure S3. Scheme of the experimental set-up. (1) influent reservoir, (2) flow-through electrochemical reactor equipped with the graphene sponge electrodes, (3) computer for the data acquisition connected to the potentiostat, (4) three electrode configuration, where the anode (working electrode), cathode (counter electrode) and leak-free Ag/AgCl as reference electrode, (5) sample collection.
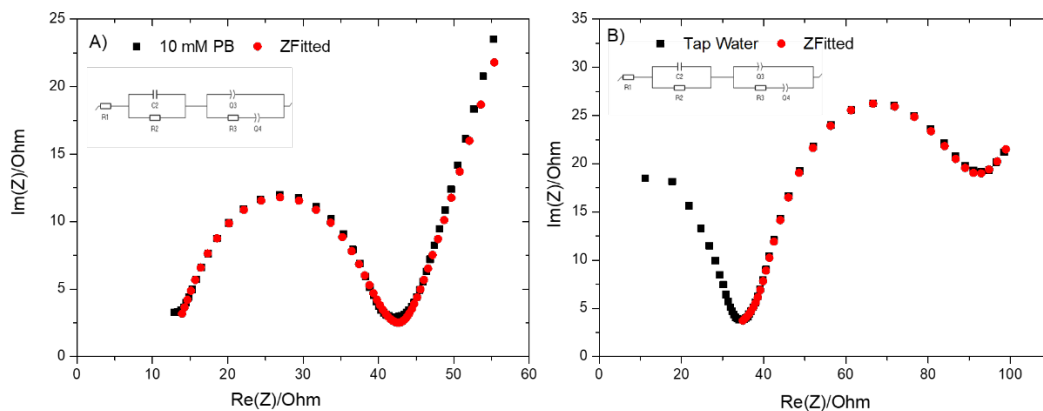
Figure S4. Nyquist diagrams of the experimental data fitted using the BioLogic EC-lab software using the equivalent circuits illustrated in the insert: **A)** 10 mM PB, and **B)** TW.

ERT, cation

OFX, zwitteronic [13]

SMX, anion[14]

TMP, neutral [6]
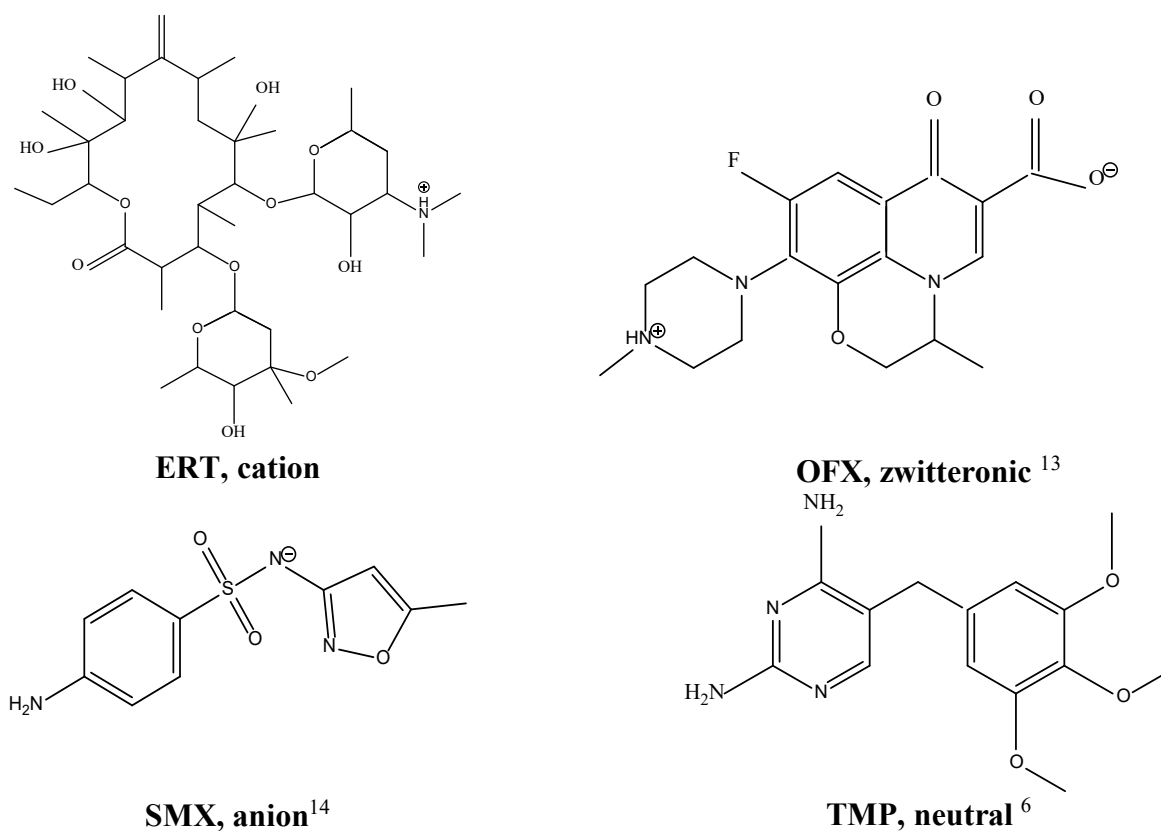
Figure S5. Chemical structures and charges of target contaminants at pH 7.
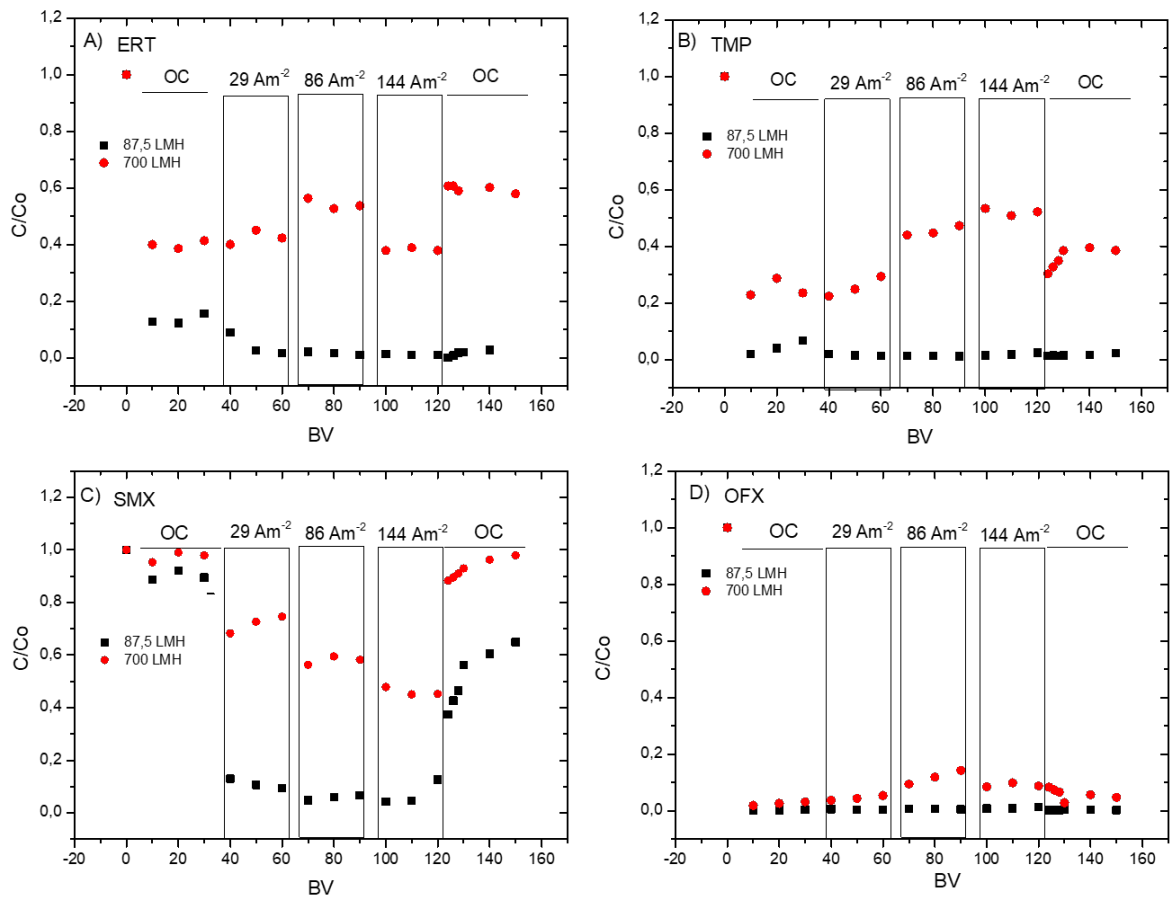
Figure S6. Effluent concentrations (C) of the target antibiotic normalized to the initial value (C_0) for the experiments conducting using 10 mM phosphate buffer at 87.5 and 700 L m^{-2} h^{-1} (LMH) for: A) ERT, B) TMP, C) SMX, and D) OFX.
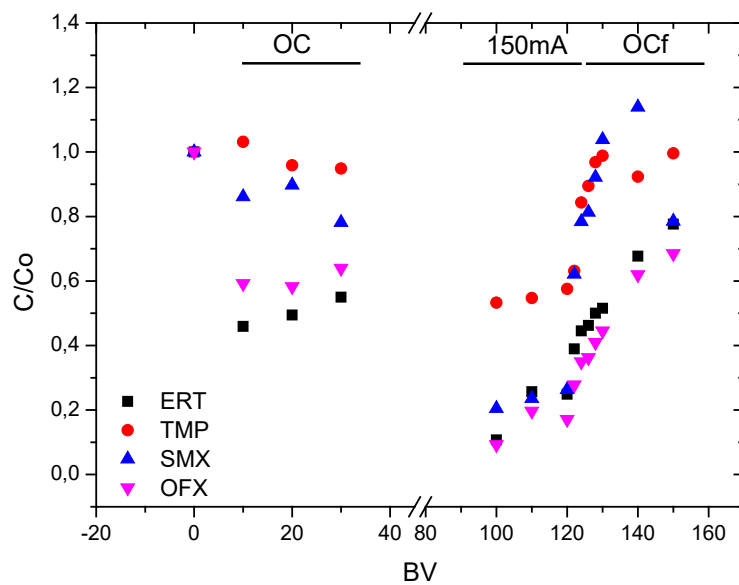
Figure S7. Concentrations (C) of the target antibiotic normalized to the initial value (C_0)

for the experiments conducting using tap water at 175 LMH.
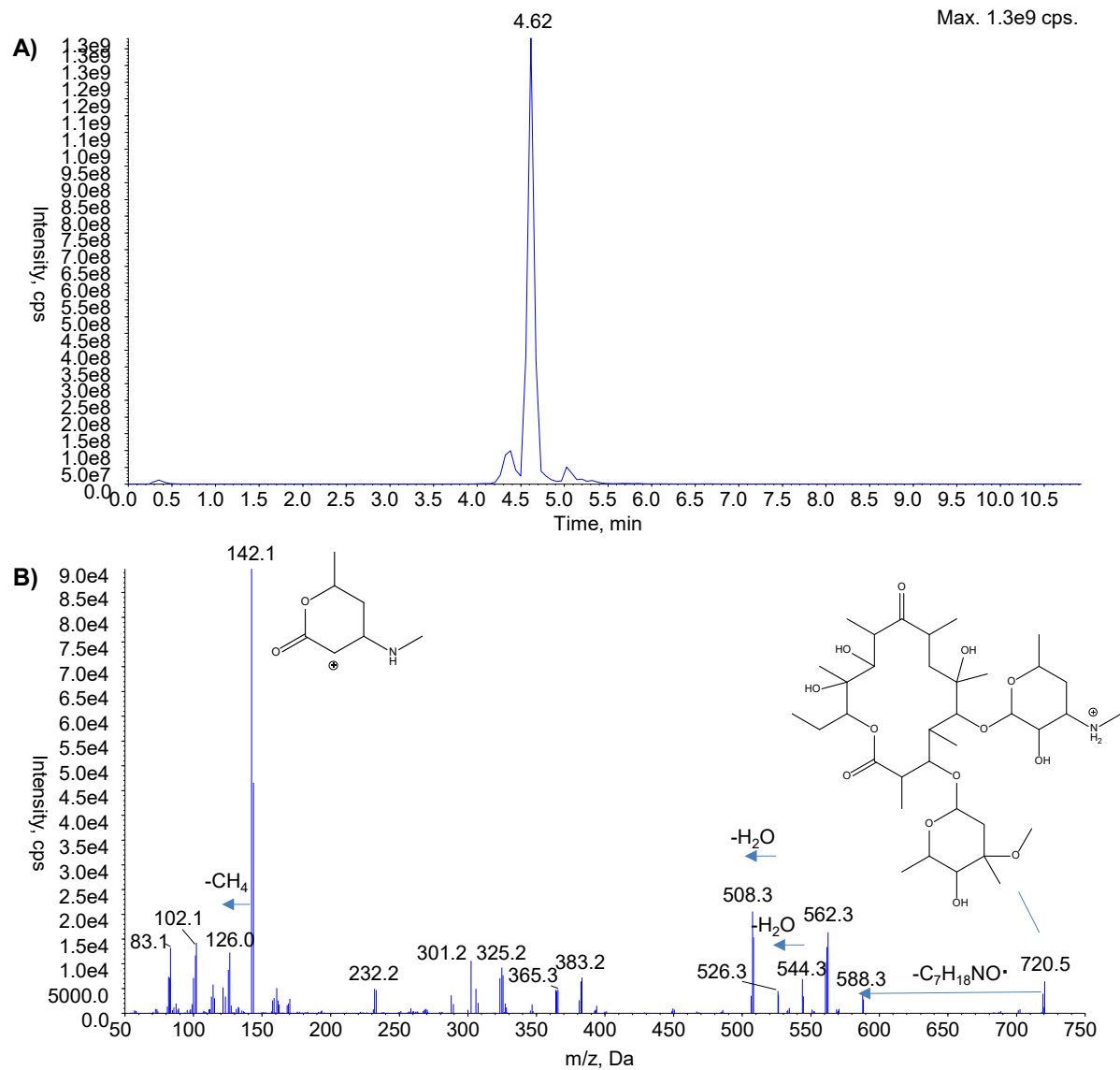
Figure S8 A) XIC of transformation product, TP720, and **B)** CID MS^2 mass spectra of the molecular ion of TP720, [M+H]$^+$ 720.4, with proposed structures and losses of fragment ions.
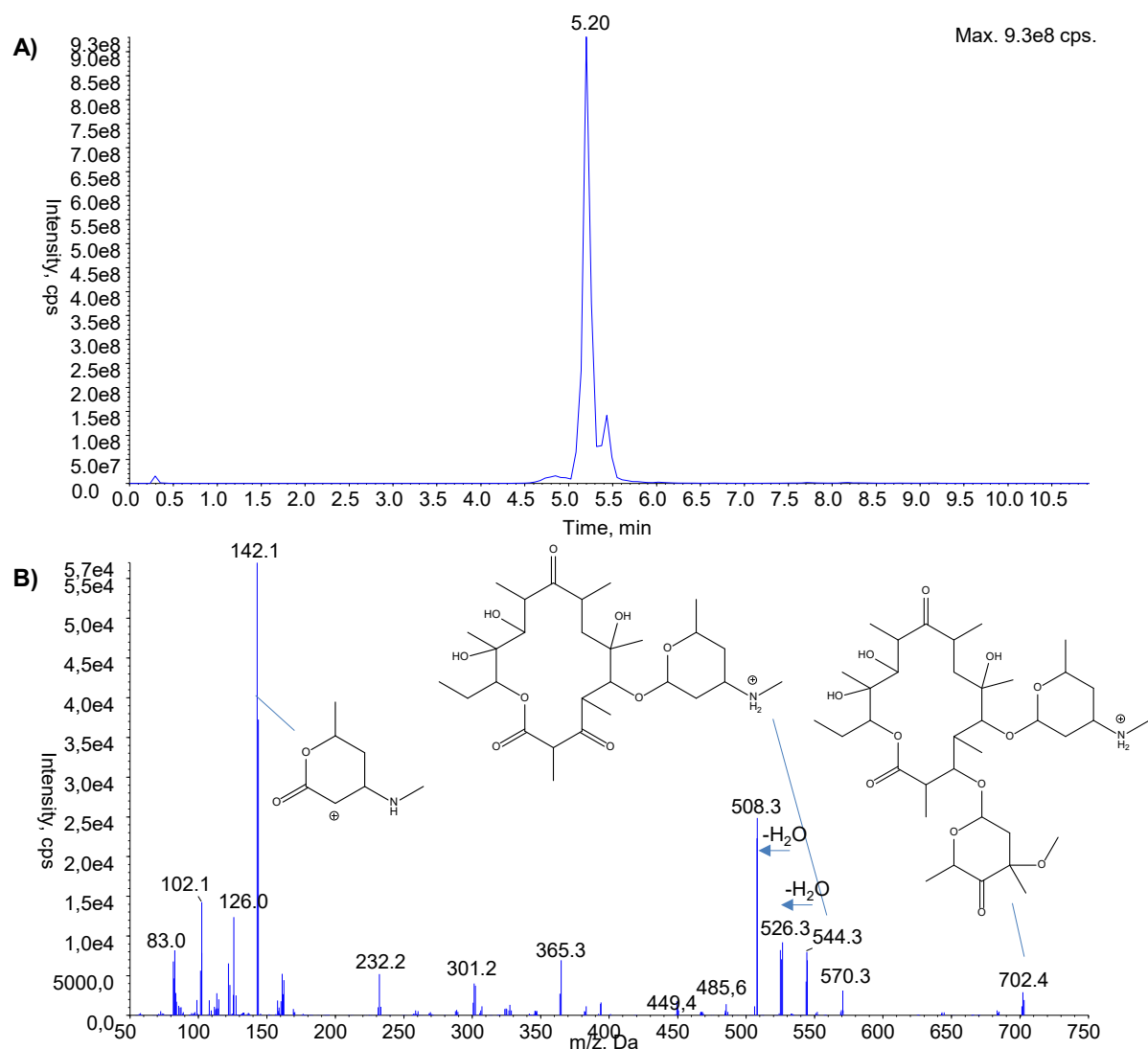
Figure S9 A) XIC of transformation product, TP702, and **B)** CID MS^2 mass spectra of the molecular ion of TP702, [M+H]$^+$ 702.4, with proposed structures and losses of fragment ions.
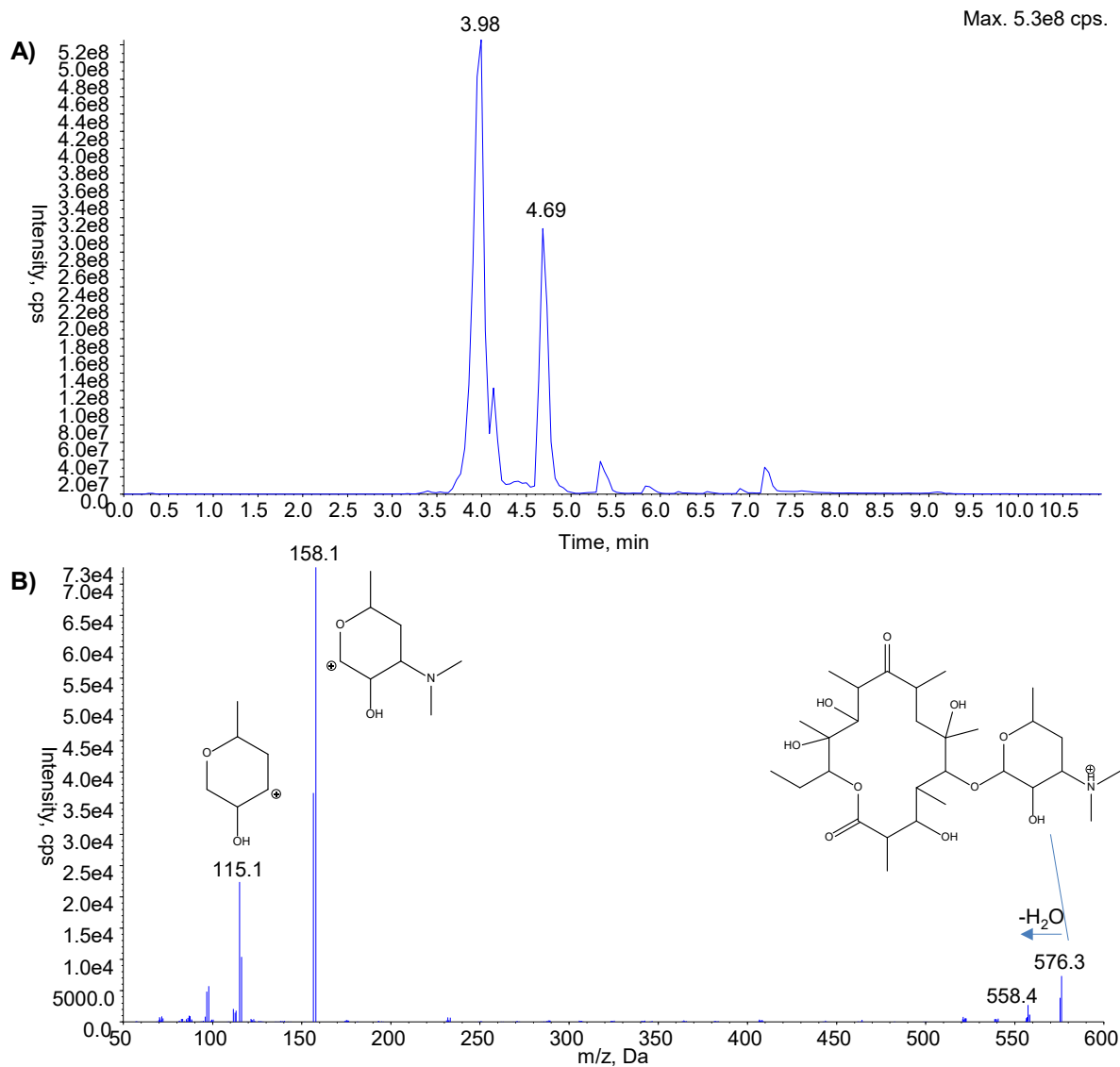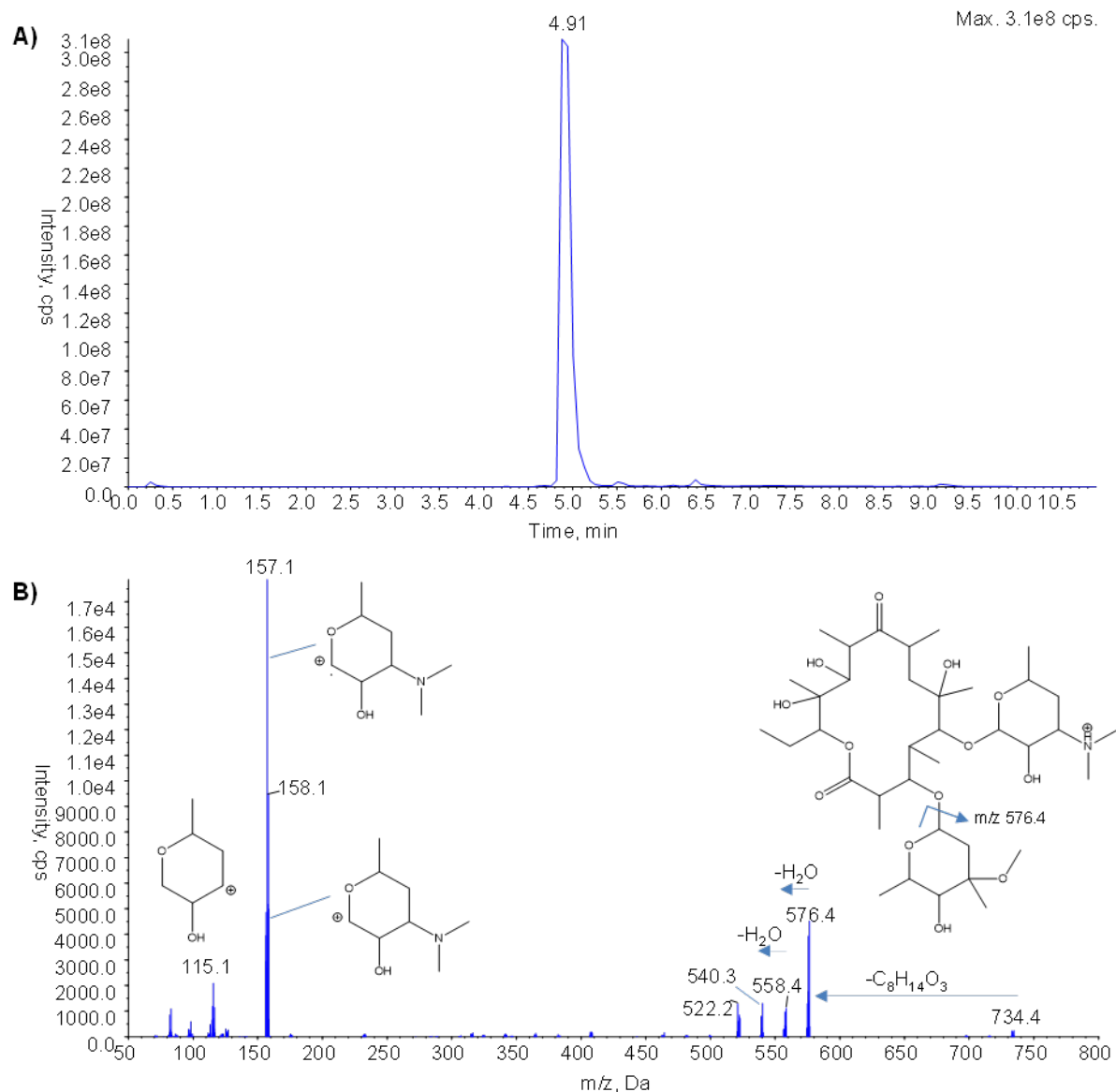
Figure S10 A) XIC of transformation product, TP576, and **B)** CID MS^2 mass spectra of the molecular ion of TP576, [M+H]$^+$ 576.3, with proposed structures and losses of fragment ions.

Figure S11 A) Extracted ion chromatograms (XIC) of erythromycin (ERT), and B) CID MS2 mass spectra of the molecular ion of ERT, $[M+H]^+$ 734.4, with proposed structures and losses of fragment ions.
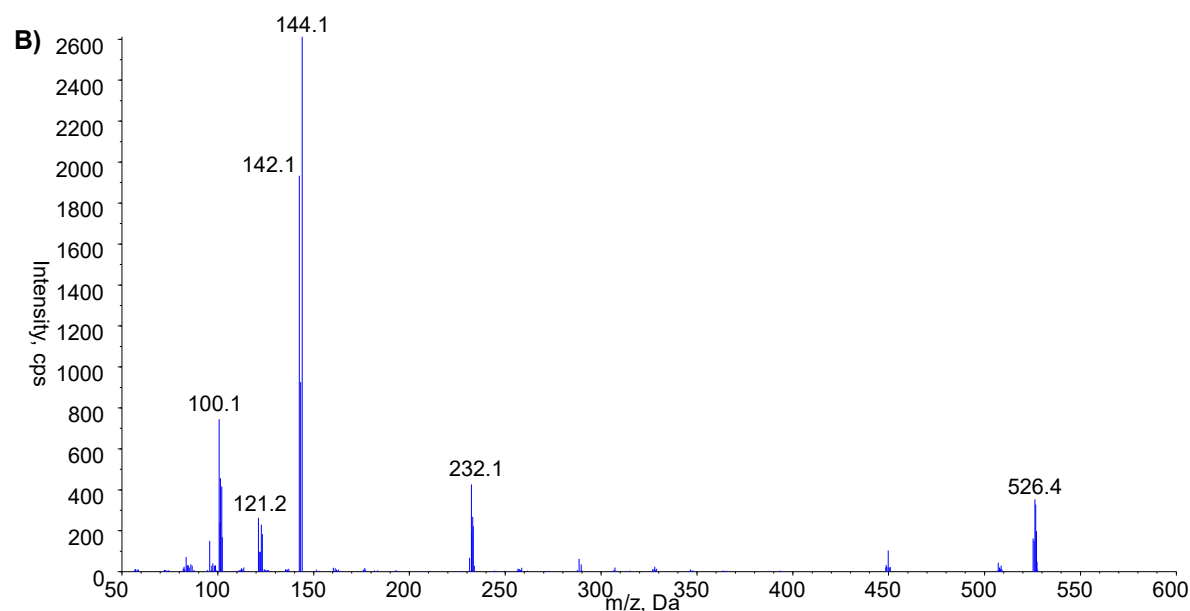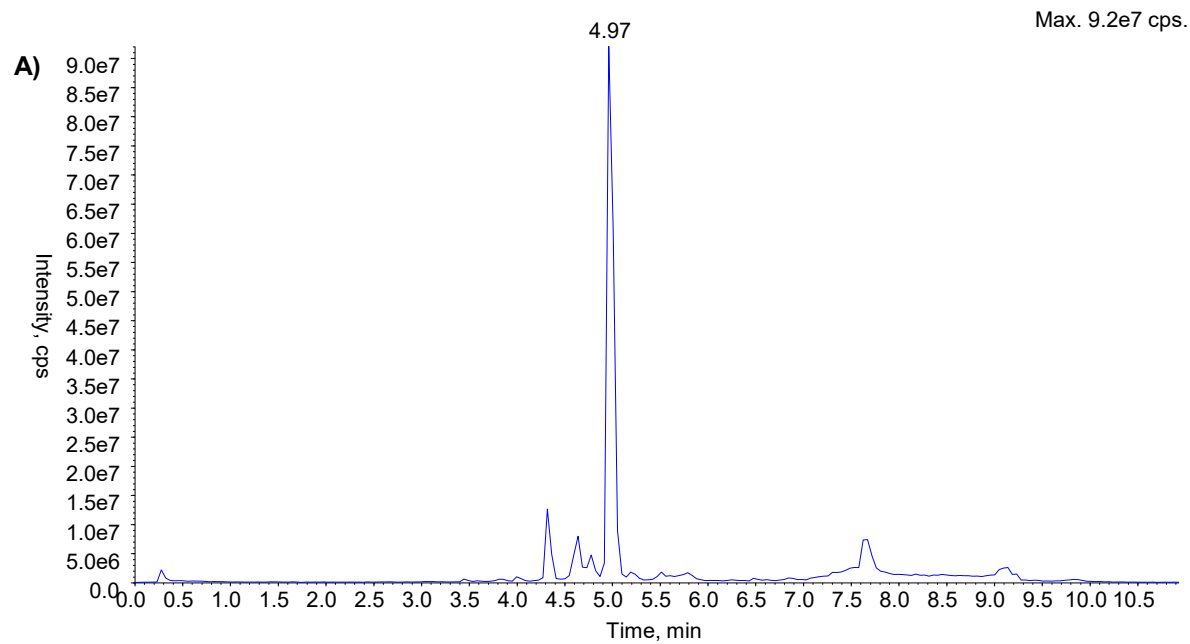
Figure S12 A) XIC of the unknown transformation product, TP526, and **B)** CID MS^2 mass spectra of the molecular ion of TP526, [M+H]$^+$ 526.5.
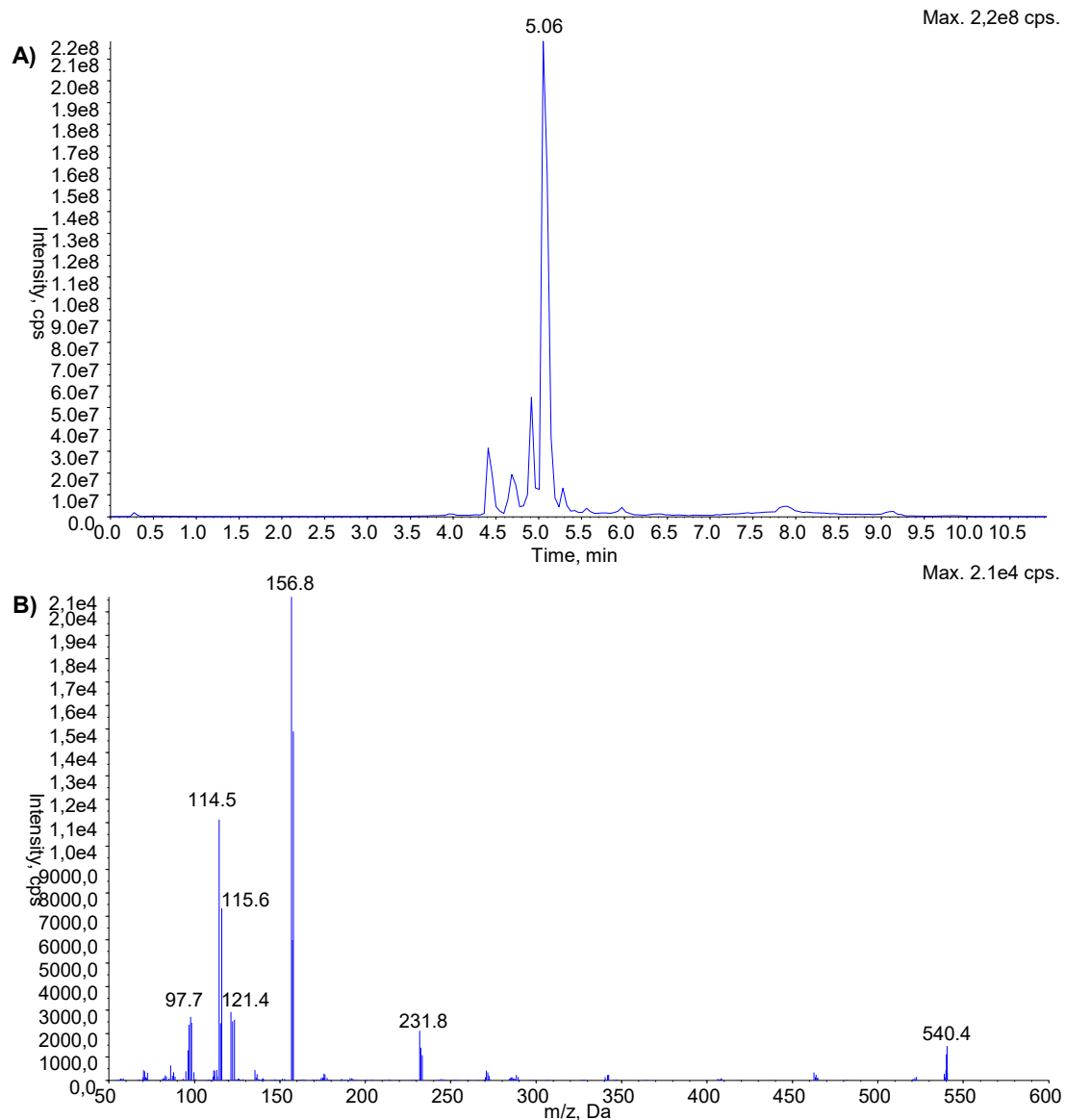
Figure S13 A) XIC of the unknown transformation product, TP540, and **B)** CID MS^2 mass spectra of the molecular ion of TP540, [M+H]$^+$ 540.4.
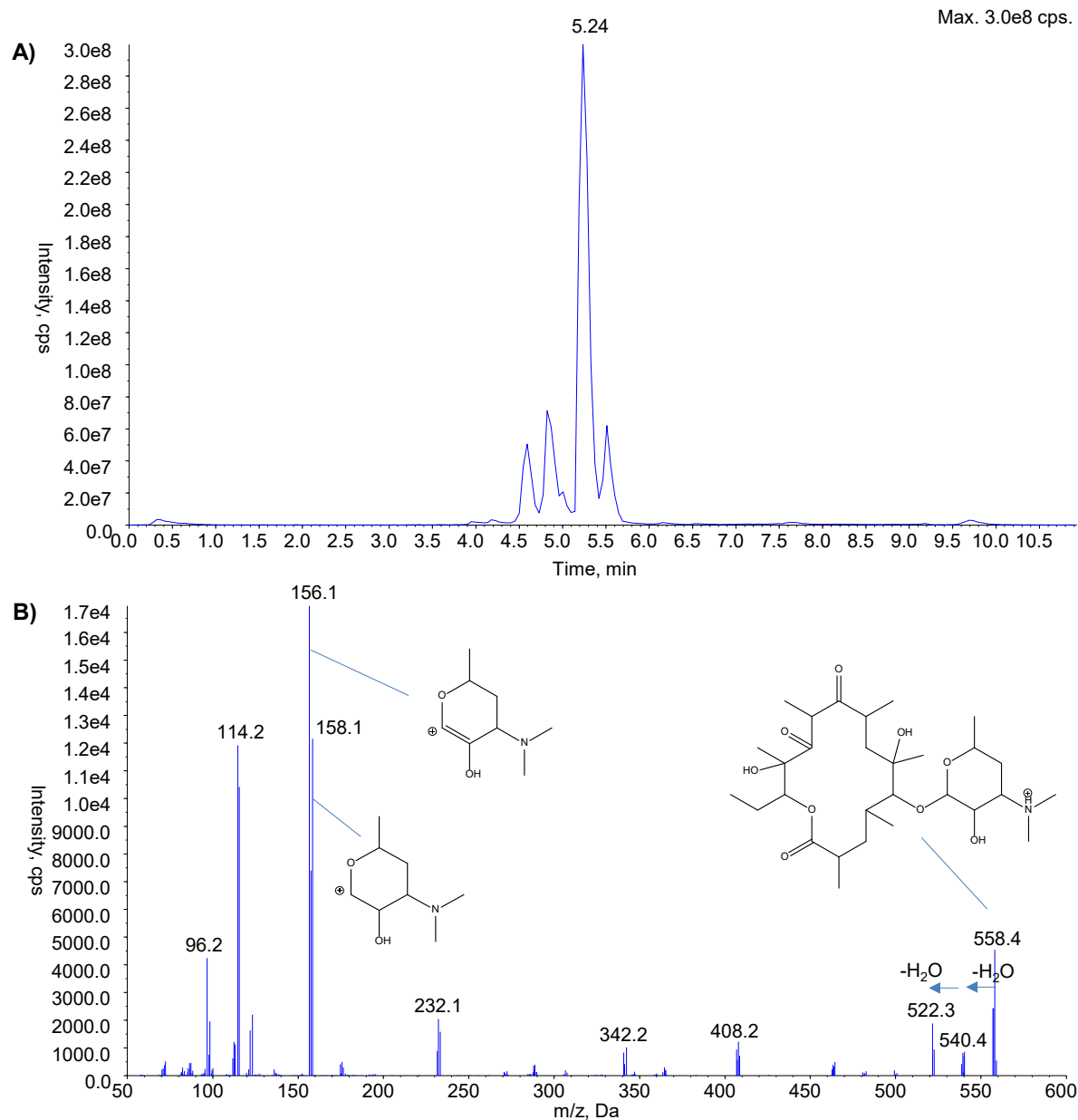
Figure S14 A) XIC of the unknown transformation product, TP558, and **B)** CID MS^2 mass spectra of the molecular ion of TP558, [M+H]$^+$ 558.4

References:

1. Baptista-Pires, L. Norra, G.-F. Radjenovic, J. Graphene Sponges for Electrochemical Degradation of Persistent Organic Contaminantss. *Water Res.* (2021).

2. Norra, G. F., Baptista-Pires, L., Cuervo Lumbaque, E., Borrego, C. M. & Radjenović, J. Chlorine-free electrochemical disinfection using graphene sponge electrodes. *Chem. Eng. J.* **430**, 132772 (2022).

3. Ge, J. *et al.* Joule-heated graphene-wrapped sponge enables fast clean-up of viscous crude-oil spill. *Nat. Nanotechnol.* **12**, 434–440 (2017).

4. Chemspider.com database(www.chemispaider.com).

5. National Center for Biotechnology Information (2021). PubChem Compound Summary for CID 5329, Sulfamethoxazole. Retrieved January 18, 2021 from https://pubchem.ncbi.nlm.nih.gov/compound/Sulfamethoxazole.

6. Radjenović, J. *et al.* Evidencing generation of persistent ozonation products of antibiotics roxithromycin and trimethoprim. *Environ. Sci. Technol.* **43**, 6808–6815 (2009).

7. Nghiem, L. D. & Hawkes, S. Effects of membrane fouling on the nanofiltration of pharmaceutically active compounds (PhACs): Mechanisms and role of membrane pore size. *Sep. Purif. Technol.* **57**, 176–184 (2007).

8. Lee, Y., Kovalova, L., McArdell, C. S. & von Gunten, U. Prediction of micropollutant elimination during ozonation of a hospital wastewater effluent. *Water Res.* **64**, 134–148 (2014).

9. Mathon, B., Coquery, M., Miege, C., Penru, Y. & Choubert, J. M. Removal efficiencies and kinetic rate constants of xenobiotics by ozonation in tertiary treatment. *Water Sci. Technol.* **75**, 2737–2746 (2017).

10. Chen, H. & Wang, J. Degradation and mineralization of ofloxacin by ozonation and peroxone (O3/H2O2) process. *Chemosphere* **269**, 128775 (2021).

11. Dodd, M. C., Buffle, M. O. & Von Gunten, U. Oxidation of antibacterial molecules by aqueous ozone: Moiety-specific reaction kinetics and application to ozone-based wastewater treatment. *Environ. Sci. Technol.* **40**, 1969–1977 (2006).

12. Wei, L. *et al.* Transformation of erythromycin during secondary effluent soil aquifer recharging: Removal contribution and degradation path. *J. Environ. Sci. (China)* **51**, 173–180 (2017).

13. Peng, H. *et al.* Adsorption of ofloxacin on carbon nanotubes: Solubility, pH and cosolvent effects. *J. Hazard. Mater.* **211**–**212**, 342–348 (2012).

14. Zhang, D. *et al.* Adsorption of sulfamethoxazole on functionalized carbon nanotubes as affected by cations and anions. *Environ. Pollut.* **159**, 2616–2621 (2011).